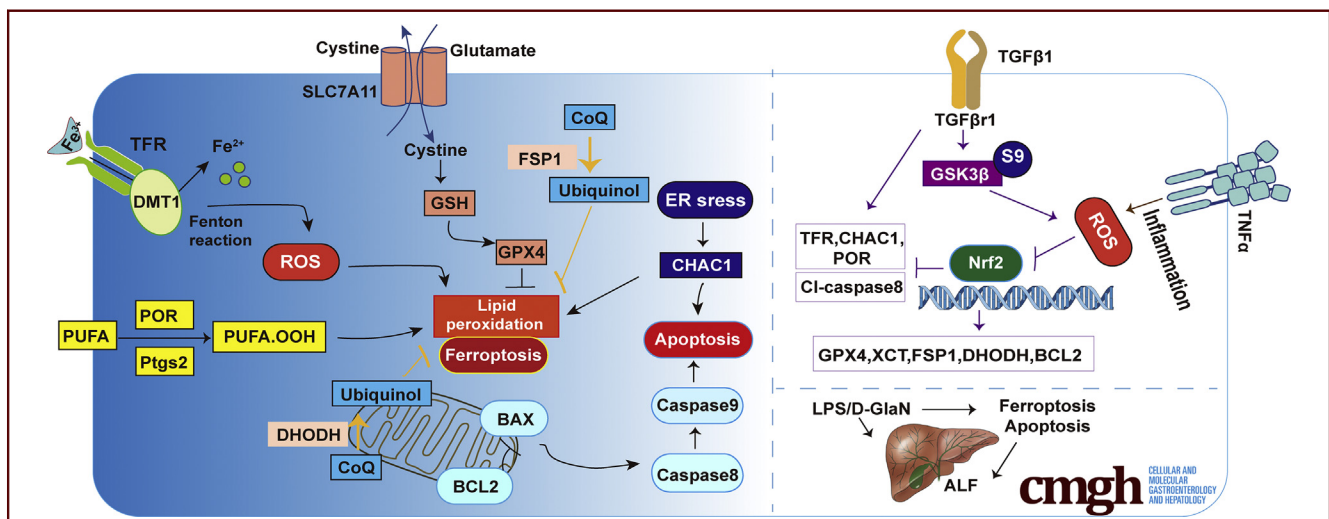


ORIGINAL RESEARCH

Hepatic TGF β 1 Deficiency Attenuates Lipopolysaccharide/
D-Galactosamine-Induced Acute Liver Failure Through Inhibiting
GSK3 β -Nrf2-Mediated Hepatocyte Apoptosis and Ferroptosis

Sha Huang,¹ Yuhua Wang,^{1,*} Shunwen Xie,¹ Yuqi Lai,² Chan Mo,³ Ting Zeng,¹ Shanshan Kuang,¹ Guanghui Deng,¹ Chuying Zhou,¹ Yuyao Chen,¹ Shaohui Huang,¹ Lei Gao,^{4,5} and Zhiping Lv¹

¹School of Traditional Chinese Medicine, Southern Medical University, Guangzhou, Guangdong, China; ²Shenzhen Traditional Chinese Medicine Hospital, Shenzhen, China; ³Medical Laboratory, Third Affiliated Hospital of Shenzhen University, Shenzhen, China; ⁴ZhuJiang Hospital of Southern Medical University, Guangzhou, Guangdong, China; and ⁵Guangdong Provincial Key Laboratory of Shock and Microcirculation, Southern Medical University, Guangzhou, Guangdong, China



SUMMARY

Apoptosis and ferroptosis contribute to lipopolysaccharide/D-galactosamine-induced acute liver failure, transforming growth factor β 1 is increased significantly during acute liver failure, and liver-specific knockout of transforming growth factor β receptor 1 alleviates lipopolysaccharide/D-galactosamine-induced acute liver failure in mice through glycogen synthase kinase 3 β -nuclear factor erythroid 2-related factor 2-mediated apoptosis and ferroptosis.

BACKGROUND & AIMS: Acute liver failure (ALF) is a condition with high mortality and morbidity, characterized by glutathione depletion, oxidative stress, and mitochondrial dysfunction. Ferroptosis may be involved in ALF. Indeed, emerging studies have shown that ferroptosis plays a significant role in ALF. However, the mechanism of ferroptosis in hepatocytes during ALF remains unknown.

METHODS: Hepatic-specific transforming growth factor β receptor 1 knockout (TGF β r1^{Δhep-CKO}) mice and nuclear factor

erythroid 2-related factor 2 knockout (Nrf2^{-/-}) mice were generated and subjected to ALF. Electron microscopy was used to detect mitochondrial and other cell substructure changes during ALF.

RESULTS: In this study, we noticed that lipopolysaccharide (LPS)/D-galactosamine (D-GalN) induced caspases-mediated apoptosis as current research reported, we also found lipid peroxidation, reactive oxygen species accumulation, and glutathione, co-enzyme Q10 system inhibition mediated ferroptosis during LPS/D-GalN-induced ALF. Rescue studies have shown that ferrostatin-1 (Fer-1) and deferoxamine mesylate (DFOM), the inhibitor of ferroptosis, could alleviate LPS/D-GalN-induced ALF. In addition, we noticed that TGF β 1 was increased during ALF, while ALF was relieved in TGF β r1^{Δhep-CKO} mice. We also noticed that liver TGF β r1 deficiency alleviated LPS/D-GalN-induced apoptosis and ferroptosis by affecting the phosphorylation of glycogen synthase kinase 3 β and Nrf2, a key antioxidant factor, by up-regulating the levels of glutathione peroxidase 4 (GPX4), glutamine antiporter xCT (XCT), dihydroorotate dehydrogenase (DHODH), and ferroptosis suppressor protein 1 (FSP1), and down-

regulating transferrin receptor (TFR), prostaglandin-endoperoxide synthase (Ptgs2), chaC glutathione specific gamma-glutamylcyclotransferase 1 (CHAC1), and cytochrome P450 reductase (POR) expression. The further supplemental experiment showed that ferroptosis was aggravated significantly in Nrf2^{-/-} mice compared with its wild-type controls and reversed by ferrostatin-1.

CONCLUSIONS: This study shows that TGFβ1 plays a critical role in mediating LPS/D-GalN-induced ALF by promoting apoptosis and ferroptosis. (*Cell Mol Gastroenterol Hepatol* 2022;13:1649–1672; <https://doi.org/10.1016/j.jcmgh.2022.02.009>)

Keywords: ALF; TGFβ1; Nrf2; GSK3β; ROS; Apoptosis; Ferroptosis.

Acute liver failure (ALF) is a condition with high mortality and morbidity that results from severe impairment of liver function induced by drugs, toxins, or viruses.¹ In western developed countries, the most common etiology is acetaminophen (APAP)-induced liver failure, in developing countries, the vast majority of cases are attributable to viral hepatitis (hepatitis A–E viruses).² If not treated in time, mortality in ALF usually results from cerebral edema or multiorgan failure. Although great progress has been made in acknowledging the molecular mechanism of ALF at present, there is still a long way to go. Because liver transplantation may be the only way to cure this disease, there is an urgent need for new treatments. ALF induced by D-galactosamine (D-GalN) and lipopolysaccharide (LPS) is a well-established experimental model, which is widely applied to search for potential therapeutics.³ LPS is the main inflammatory bacterial component by triggering the activation of immune cells and initiating the inflammation response, while D-GalN is responsible for sensitizing to LPS lethality by inhibiting protein and RNA synthesis by depleting uridine triphosphate (UTP), primarily in the liver.^{4,5}


ALF is interlinked with various factors such as oxidative stress, apoptosis, and inflammation. Reactive oxygen/nitrogen species and expression of death ligands in the process culminating in hepatocyte death are well documented and most of the current studies attribute hepatocyte death to apoptosis.⁶ Ferroptosis characterized by accumulation of reactive oxygen species (ROS) and iron accumulation, and the release of damage-associated molecular patterns, plays an important role in liver disease, including acute liver injury and liver fibrosis.^{7–9} The imbalance between excess production of ROS and the body's ability to neutralize or eliminate its harmful effects through antioxidants such as glutathione (GSH) and coenzyme Q10 (CoQ10) result in oxidative damage.¹⁰ Specifically, glutathione peroxidase 4 (GPX4) is a main regulator of the GSH antioxidant system and prevents ferroptosis by converting lipid hydroperoxides into nontoxic lipid alcohols.¹¹ Ferroptosis suppressor protein 1 (FSP1) acts as an oxidoreductase that reduces ubiquinone to ubiquinol mainly on the plasma membrane while dihydroorotate dehydrogenase (DHODH) inhibits ferroptosis in the mitochondrial inner membrane by reducing

ubiquinone to ubiquinol.^{12,13} However, how the ferroptosis reacts to ALF remains largely obscure. Former studies have described that malondialdehyde (MDA) levels are increased in LPS/D-GalN-induced acute liver injury.¹⁴ Other research has shown that ferroptosis is related to acetaminophen (APAP)-induced hepatocyte cell death, which indicates that ferroptosis plays a significant role in ALF and further research needs to be conducted.¹⁵ Nuclear factor E2-related factor 2 (Nrf2) is the major regulator of the cellular antioxidant response and participates in the regulation of ferroptosis. Certain studies have found that activation of Nrf2 attenuates LPS/D-GalN-induced acute liver injury and reduces ferroptosis.¹⁶ Glycogen synthase kinase 3β (GSK3β) is an indispensable regulator of the oxidative stress response. A multitude of evidence suggests that GSK3β regulation of Nrf2 is implicated in aging, acute liver injury, hepatotoxicity, and neurologic degeneration. In chronic hepatitis C, the expression of phosphorylated GSK3β correlated positively with Nrf2 expression and was associated inversely with the degree of liver injury, the inhibitory effect of GSK3β on Nrf2 is promoted with transforming growth factor β1 (TGFβ1).¹⁷ Nevertheless, very little was known about how TGFβ1 regulates GSK3β by affecting Nrf2 antioxidant response in ferroptosis-induced acute liver injury.

TGFβ, produced by many cell types, including non-parenchymal cells in the liver, similar to liver macrophages, plays important roles in the processes of ALF.¹⁸ TGFβ mediates their signaling via a specific complex of type I/type II receptor serine/threonine kinases and plays a significant role in cell proliferation, differentiation, migration, and cell death. Previous clinical research has shown that the expression of TGFβ1 is increased in ALF patients because TGFβ1 inhibits hepatic DNA synthesis and reduces liver

*Authors share co-first authorship.

Abbreviations used in this paper: AAV9, adeno-associated virus serotype 9; ALF, acute liver failure; ALT, alanine aminotransferase; AST, aspartate aminotransferase; APAP, acetaminophen; BAX, bcl-2 associated X; BCL2, b-cell lymphoma 2; CHAC1, ChaC glutathione specific gamma-glutamylcyclotransferase 1; CoQ10, coenzyme Q10; DFOM, deferoxamine mesylate; DHODH, dihydroorotate dehydrogenase (quinone); DMT1, divalent Metal Transporter 1; Fer-1, ferrostatin-1; FSP1, ferroptosis suppressor protein 1; GalN, galactosamine; GPX4, glutathione peroxidase 4; GSDMD, gasdermin D; GSH, glutathione; GSK3β, glycogen synthase kinase 3β; iNOS, inducible nitric oxide synthase; LPS, lipopolysaccharide; MDA, malondialdehyde; NC, negative control; Nfe2l2, NFE2 like bZIP transcription factor 2; NO, nitric oxide; Nrf2, nuclear factor erythroid 2-related factor 2; NT, Nitrotyrosine; PBS, phosphate-buffered saline; POR, cytochrome P450 Reductase; Ptgs2, prostaglandin-endoperoxide synthase 2; PUFA, polyunsaturated fatty acid; RIP3, receptor-interacting protein 3; RNAi, RNA interference; ROS, reactive oxygen species; SOD, Superoxide dismutase; TFR, transferrin receptor; TGFβ1, transforming growth factor β1; TGFβ1, transforming growth factor β receptor 1; TGFβ1^{Δhep-cko}, liver-specific transforming growth factor β receptor 1 knockout; TNFα, tumor necrosis factor α; TUNEL, terminal deoxynucleotidyl transferase-mediated deoxyuridine triphosphate nick-end labeling; WT, wild-type; XCT, Glutamine antiporter xCT; ZAVD-FMK, Z-VAD(OMe)-FMK; 4-HNE, 4-hydroxynonenal.

 Most current article

© 2022 The Authors. Published by Elsevier Inc. on behalf of the AGA Institute. This is an open access article under the CC BY-NC-ND license (<http://creativecommons.org/licenses/by-nc-nd/4.0/>).

2352-345X

<https://doi.org/10.1016/j.jcmgh.2022.02.009>

regeneration.^{19,20} Another study also showed that inhibition of TGF β receptor 1 (TGF β 1) improves mouse survival in APAP poisoning.²¹ Increases in circulating TGF β 1 level also have been described in patients with systemic inflammatory response syndrome (SIRS), an important syndrome of ALF.²² There is no evidence, however, indicating a pathogenic role of TGF β 1 in ALF. It is necessary to study the regulatory mechanism of TGF β 1 in ALF from a new perspective. Therefore, this study examined the regulatory effect of TGF β 1 on ferroptosis in ALF. We established LPS/D-GalN-induced ALF as an experimental model and found that ferroptosis was enhanced in LPS/D-GalN-induced ALF, while deletion of hepatic TGF β 1 relieved LPS/D-GalN-induced ALF by inhibiting apoptosis and ferroptosis through regulating GSK3 β -Nrf2.

Results

ALF Resulted in Hepatocellular Apoptosis and Ferroptosis

We first established the LPS/D-GalN-induced ALF model by intraperitoneally injecting mice with LPS (20 μ g/kg) 15 minutes before injection of D-GalN (700 mg/kg) and examined the survival rate and liver function. As shown in Figure 1A and B, liver tissues were harvested 6 hours after LPS/D-GalN injection because we found that mice began to die 5 hours after LPS/D-GalN injection, and the survival rate of mice dropped to approximately 0%–20% in 6 hours. The level of alanine aminotransferase (ALT) and aspartate aminotransferase (AST) of mice with LPS/D-GalN treatment was sharply increased compared with control mice (Figure 1C). Furthermore, H&E and terminal deoxynucleotidyl transferase-mediated deoxyuridine triphosphate nick-end labeling (TUNEL) staining of liver sections showed that extensive destruction of liver structure, diffuse hemorrhagic necrosis, and combined severe liver congestion and hepatocyte apoptosis were seen in the mouse liver with LPS/D-GalN treatment, compared with the observations in control mice (Figure 1D). With LPS/D-GalN injection, tumor necrosis factor α (TNF α) was activated as well as intrahepatic inflammatory cells such as macrophages and neutrophils. They were detected by TNF α , F4/80, and lymphocyte antigen 6 complexes, locus G (LY6G) immunohistochemistry, and were increased significantly, as compared with the results in control mice (Figures 1E and Figure 2A). As reported in previous studies,²³ apoptosis plays an important role in LPS/D-GalN-induced ALF. We also detected the activation of caspase proteins such as caspase 8 and caspase 9, as well as the activation of the b-cell lymphoma 2 (BCL2)-BAX system (Figure 2B and C).

Next, we detected the mitochondrial changes in the liver by electron microscopy and surprisingly found that mitochondria appeared smaller than the control group, with increased membrane density, which was the main feature of ferroptosis (Figure 1F). To further evaluate the role of ferroptosis induced by LPS/D-GalN, we assessed lipid peroxidation and iron metabolism. Because polyunsaturated fatty acids (PUFAs) are the main substrates of lipid peroxidation in the process of ferroptosis, cytochrome P450 reductase

(POR) and prostaglandin-endoperoxide synthase 2 (Ptgs2), mediating the formation of PUFAs from PUFAs hydrolyzed peroxy radical (OOH), plays a significant role in lipid peroxidation. With Western blot assay, we found the expression of POR and Ptgs2 were low in the control liver, although significantly increased after LPS/D-GalN administration (Figure 1I and L). MDA, a lipid peroxidation product, also was triggered significantly after the treatment of LPS/D-GalN (Figure 1G). The main anti-ferroptosis activity of the GSH system is related to GPX4 and glutamine antiporter xCT (XCT), and the expression of GPX4 and XCT was decreased after LPS/D-GalN treatment (Figure 1H). As another antioxidant, DHODH and FSP1 can mediate the production of CoQ10 to inhibit ferroptosis in a GSH-independent manner. The expression of DHODH and FSP1 were also inhibited after LPS/D-GalN treatment (Figure 1J). For iron metabolism, we mainly detected changes in Fe $^{2+}$ levels and related proteins such as transferrin receptor (TFR) and divalent metal transporter 1 (DMT1).²⁴ Compared with the control group, the plasma Fe $^{2+}$ level (Figure 5C) was increased significantly, as well as the expression of TFR and DMT1 after LPS/D-GalN treatment (Figure 1H and L).

Taken together, these results suggest both apoptosis and ferroptosis occurred in LPS/D-GalN-induced ALF. In-depth exploration of the mechanism of ferroptosis in ALF may provide new ideas for clinical practice.

Inhibition of Apoptosis or Ferroptosis Attenuated LPS/D-GalN-Induced ALF

In the earlier-described experiments, we found that both apoptosis and ferroptosis occurred in ALF. Next, we respectively injected mice with apoptosis inhibitor ZAVD-FMK (10 mg/kg) and ferroptosis inhibitor ferrostatin-1 (Fer-1) (10 mg/kg) and deferoxamine mesylate (DFOM) (100 mg/kg) 1 hour before LPS/D-GalN administration to see if they could save mice from ALF. Both apoptosis and ferroptosis inhibitors could prolong the mice's survival rate (Figures 3A and 5A).

ZAVD-FMK is an irreversible pan-caspase inhibitor. In our research, compared with the LPS/D-GalN group, we found that the levels of ALT and AST were decreased with ZAVD-FMK treatment (Figure 3B). Sections of livers from the LPS/D-GalN group showed pathologic damage and numerous apoptotic hepatocytes while showing less hepatic congestion and fewer apoptotic hepatocytes (Figure 3C). The GSH and MDA assays of liver tissue homogenates showed that the LPS/D-GalN group showed a lower level of GSH and a high level of MDA, while the ZAVD-FMK+LPS/D-GalN group could increase the GSH level and reduce the MDA level (Figure 3D and E). Both caspases and BCL2-BAX were activated during LPS/D-GalN-induced ALF. Specifically, BCL2 was inhibited while caspase 9 (Aspartate 368,39 kDa, P39) and cleaved caspase 8 were increased, and there were no significant changes in the expression of caspase 8. With ZAVD-FMK treatment, the expression of BCL2 was increased while the expression of caspase 9 and cleaved caspase 8 was decreased (Figure 3F and G).

Fer-1, a potent inhibitor of ferroptosis, has been shown to suppress ferroptosis in cells and a mammalian model

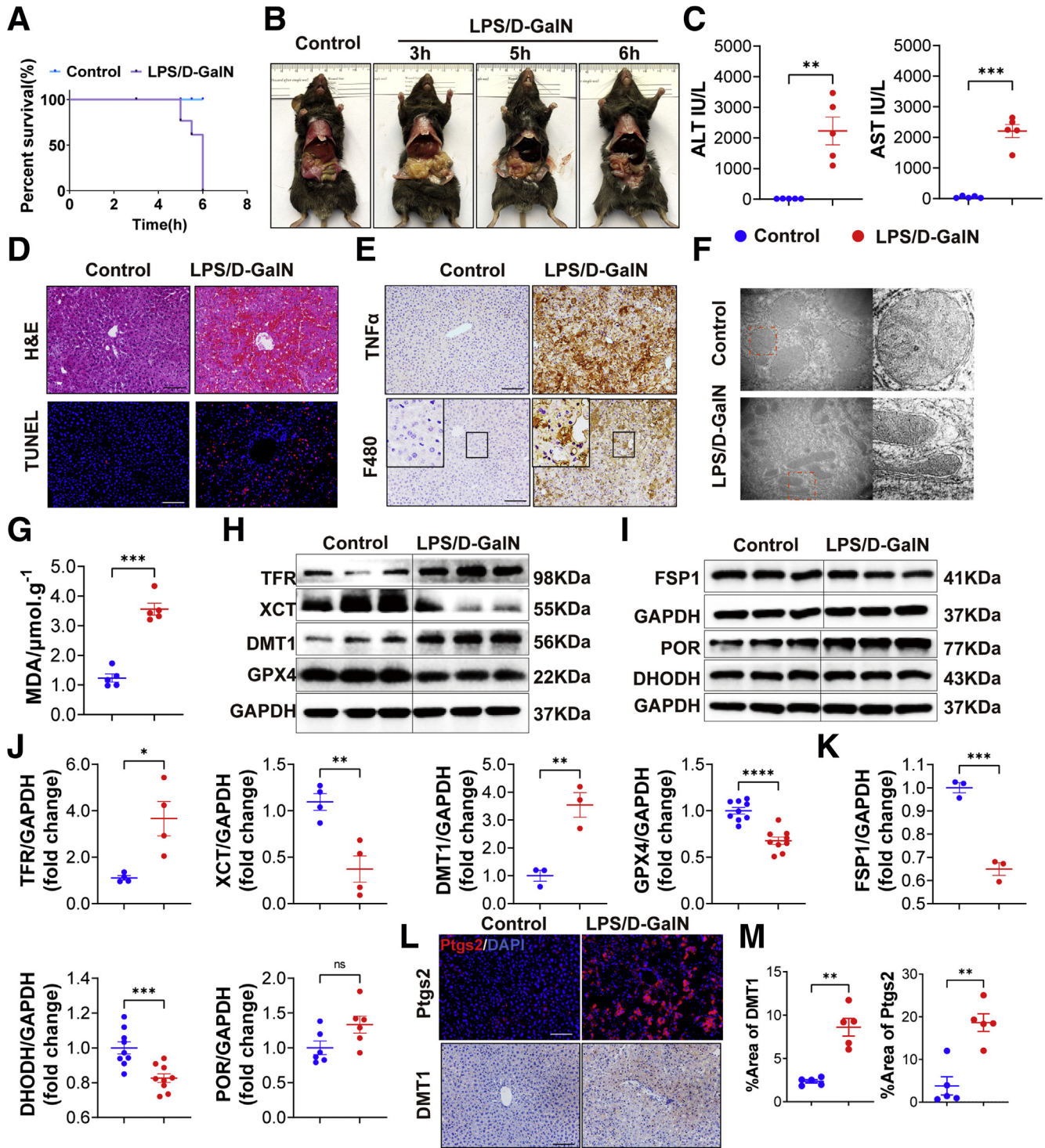


Figure 1. LPS/D-GalN-induced ALF enhances apoptosis and ferroptosis. (A) The survival rate of WT mice treated with vehicle or LPS/D-GalN (LPS, 20 $\mu\text{g}/\text{kg}$; D-GalN, 700 mg/kg) ($n = 10$). (B) Representative pictures of WT mice treated with vehicle or LPS/D-GalN for 3, 5, and 6 hours ($n = 10$). (C) Serum levels of ALT and AST with or without LPS/D-GalN co-injection ($n = 6$). (D) H&E and TUNEL staining after LPS/D-GalN co-injection ($n = 6$). (E) Immunohistochemistry of TNF α and F4/80 staining after LPS/D-GalN co-injection ($n = 6$). (F) Transmission electron microscope of liver tissues ($n = 3$). (G) MDA assay of liver homogenates ($n = 5$). (H and J) Western blot analyses of TFR, DMT1, GPX4, and XCT from WT mice (H) with or without LPS/D-GalN and (J) quantitative results ($n = 3-9$). (I and K) FSP1, DHODH, and POR proteins. Western blot analyses of WT mice (I) with or without LPS/D-GalN and (K) quantitative results ($n = 3-9$). (L) Immunohistochemistry of DMT1 staining and immunofluorescence of Ptg2 in livers with or without LPS/D-GalN ($n = 6$). (M) Quantitative results of DMT1 and Ptg2. All data were obtained from WT mice. Scale bars: 100 μm . Data are presented as means \pm SEM. * $P < 0.05$, ** $P < 0.01$, *** $P < 0.001$, **** $P < 0.0001$. DAPI, 4',6-diamidino-2-phenylindole; GAPDH, glyceraldehyde-3-phosphate dehydrogenase.

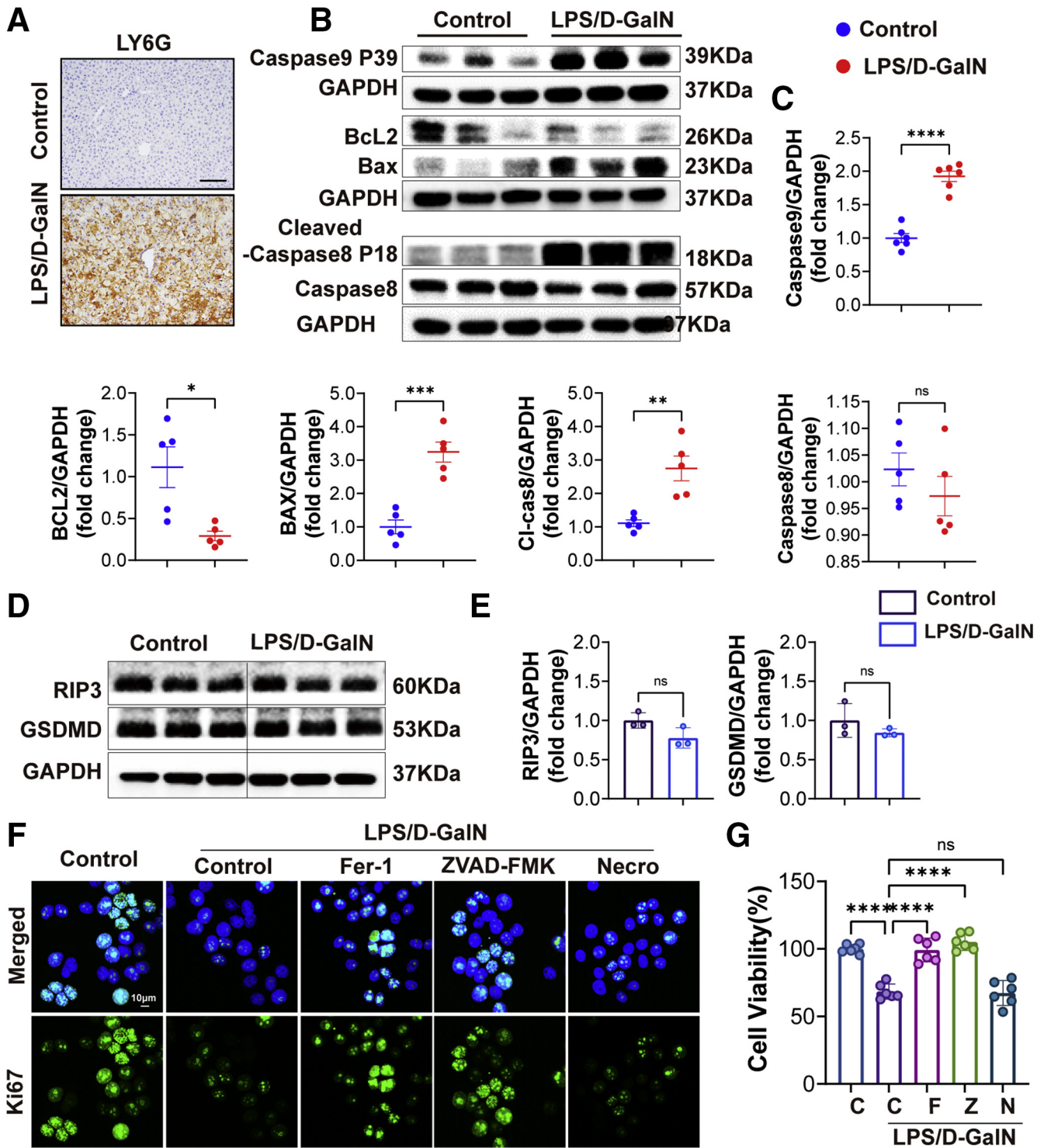


Figure 2. Apoptosis was increased during LPS/D-GalN-induced ALF. (A) LY6G immunohistochemistry staining of WT mice with or without LPS/D-GalN treatment. Scale bars: 100 μm. (B) Western blot analyses of caspase 9, BCL2, BAX, caspase 8, and cl-caspase 8 (cleaved-caspase 8) proteins from WT mouse liver treated with or without LPS/D-GalN co-injection (n = 5–6). (C) Quantitative results of caspase 9, BCL2, BAX, caspase 8, and cl-caspase 8. (D) Western blot analyses of RIP3 and GSDMD from WT mouse liver treated with or without LPS/D-GalN co-injection. (E) ratios of each protein to GAPDH (n = 3). (F) Ki67 immunofluorescence staining of L02 with or without LPS/D-GalN (LPS, 10 ng/mL; D-GalN, 1 mmol/L). (G) Cell Counting Kit-8 (CCK8) assay of LPS/D-GalN induced L02 injury pretreated with Fer-1 (1 μmol/L), ZVAD-FMK (10 μmol/L), and Nec-1 (10 μmol/L) (n = 5). Scale bar: 10 μm. Data are presented as means ± SEM. *P < 0.05, **P < 0.01, ***P < 0.001, ****P < 0.0001. C, Control; F, Fer-1; GAPDH, glyceraldehyde-3-phosphate dehydrogenase; N, Necrostatin-1; Z, ZVAD-FMK.

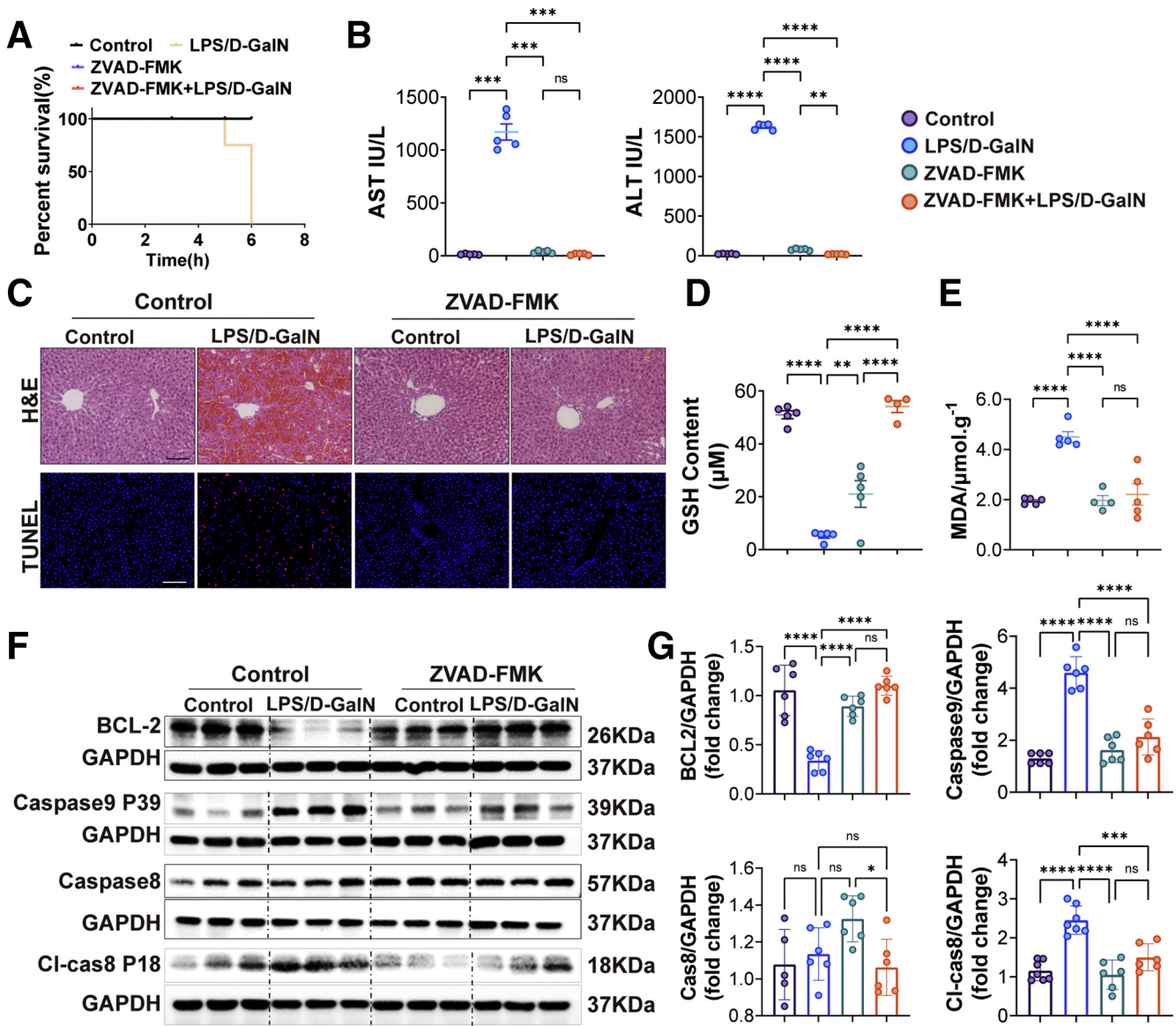


Figure 3. ZVAD-FMK relieved LPS/D-GalN-induced ALF through inhibiting apoptosis. (A) The survival rate of WT mouse liver treated with vehicle or ZVAD-FMK (10 mg/kg) 1 hour before LPS/D-GalN co-injection (n = 5). (B) Serum levels of ALT and AST. (C) H&E and TUNEL staining of mouse liver treated with vehicle or ZVAD-FMK before LPS/D-GalN co-injection (n = 6). (D and E) GSH and MDA assay of liver homogenates (n = 5). (F) Western blot analyses of BCL2, caspase 9, caspase 8, and cleaved (cl)-caspase 8 proteins. (G) Quantitative results of BCL2, caspase 9, caspase 8, and cl-caspase 8 proteins (n = 6). All data were obtained from WT mice. Scale bar: 100 μm. Data are presented as means ± SEM. *P < 0.05, **P < 0.01, ***P < 0.001, ****P < 0.0001. D-GalN, D-galactosamine; GAPDH, glyceraldehyde-3-phosphate dehydrogenase.

with acute liver injury in our previous research.^{7,8} The main mechanism by which Fer-1 inhibits ferroptosis is the inhibition of ROS accumulation caused by lipid peroxidation.²⁵ Treatment with Fer-1 significantly suppressed the increase in the levels of ALT and AST of mice with LPS/D-GalN treatment (Figure 4B), consistent with H&E and TUNEL staining. Fer-1 attenuated liver congestion and reduced scattered hepatocyte death including apoptosis (Figure 4A). The level of MDA was reduced after treatment with Fer-1 (Figure 4C). Then we detected the expression of Ptg2 and 4-hydroxynonenal (4-HNE) (the marker of lipid peroxidation) by immunochemical staining and found the levels of

Ptg2 and 4-HNE were decreased significantly with Fer-1 treatment (Figure 4H and I). GPX4, protecting cells against membrane lipid peroxidation and cell death, was detected by Western blot and immunofluorescence staining and rescued by Fer-1 treatment after LPS/D-GalN injection (Figure 4D and F). We also detected the expression of DMT1 and found that DMT1 was decreased significantly with Fer-1 treatment (Figure 4F).

DFOM is the mesylate salt of deferoxamine, which forms an iron complex and acts as a chelating agent, and used as a ferroptosis inhibitor. Similar to previous detection methods, DFOM could decrease the levels of ALT and AST and

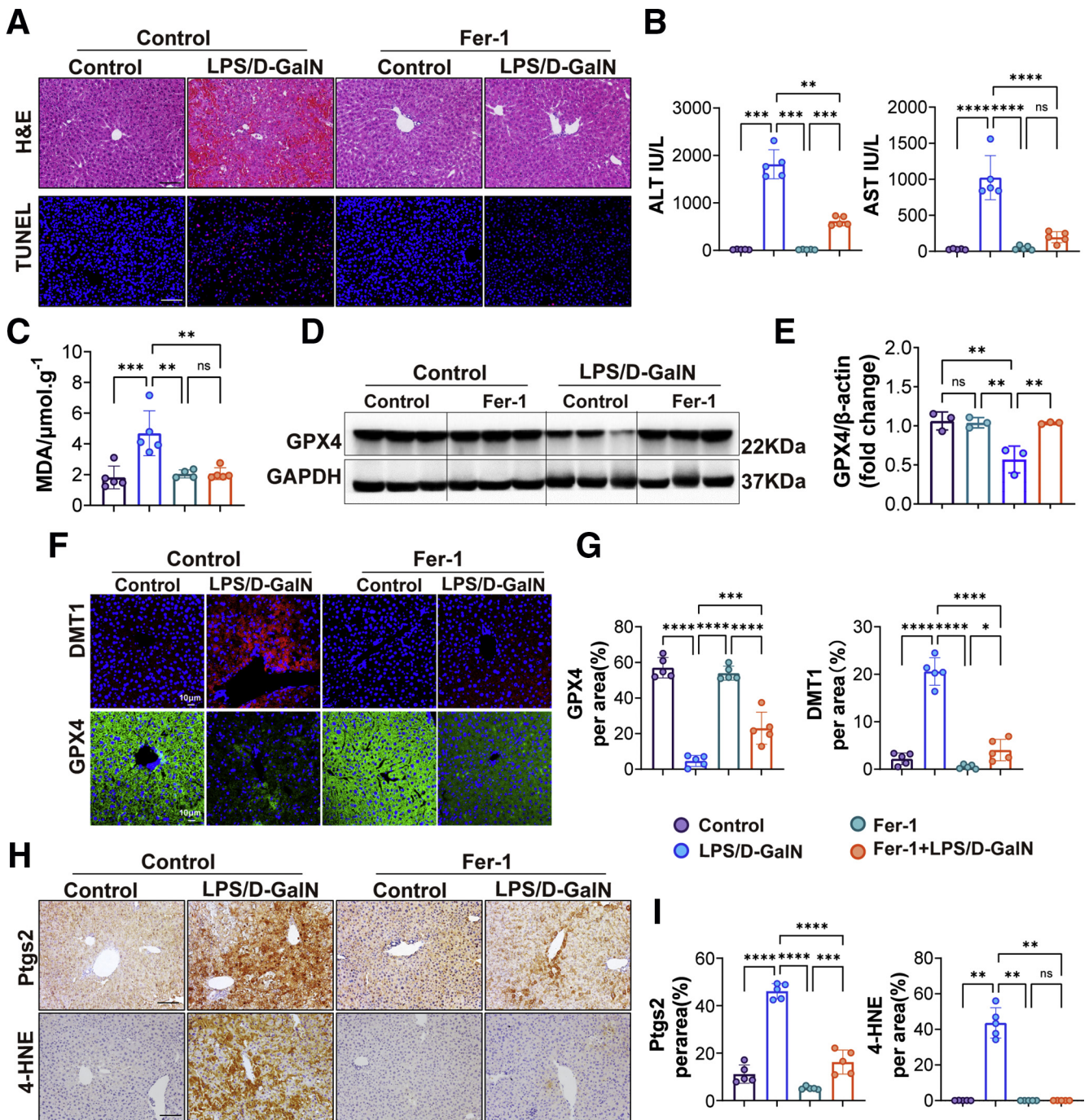


Figure 4. Fer-1 attenuated LPS/D-GalN-induced ALF by repressing ferroptosis. (A) Representative pictures for H&E and TUNEL staining from WT mice treated with vehicle or Fer-1 (10 mg/kg) 1 hour before LPS/D-GalN treatment ($n = 5$). Scale bars: 100 μm . (B) Serum levels of ALT and AST from WT mice treated with vehicle or Fer-1 before LPS/D-GalN treatment ($n = 5$). (C) MDA assay of liver homogenate from WT mice treated with vehicle or Fer-1 before LPS/D-GalN treatment ($n = 5$). (D) Representative GPX4 Western blots of WT mice treated with vehicle or Fer-1 before LPS/D-GalN treatment and (E) quantitative results of GPX4/ β -actin ($n = 3$). (F) Immunofluorescence of DMT1 and GPX4 staining of WT mice treated with vehicle or Fer-1 before LPS/D-GalN treatment and (G) quantitative results ($n = 5$). Scale bars: 10 μm . (H) Ptgs2 and 4-HNE immunohistochemistry staining of WT mice treated with vehicle or Fer-1 before LPS/D-GalN treatment and (I) quantitative results ($n = 5$). Scale bars: 100 μm . All data were obtained from WT mice. Data are presented as means \pm SEM. * $P < 0.05$, ** $P < 0.01$, *** $P < 0.001$, **** $P < 0.0001$. D-GalN, D-galactosamine; GAPDH, glyceraldehyde-3-phosphate dehydrogenase.

attenuated liver congestion, and reduced scattered hepatocyte death in LPS/D-GalN-induced ALF (Figure 5B and D). DFOM also could increase the level of GSH and decrease the level of MDA (Figure 5E and F). However, as TUNEL staining showed in Figure 5D, the difference was that DFOM did not reduce apoptosis of hepatocytes, which indicated that DFOM could not inhibit apoptosis. We also found that DFOM could decrease the level of Fe^{2+} (Figure 5C). Then, we tested the multiple proteins related to ferroptosis. ChaC glutathione specific gamma-glutamylcyclotransferase 1 (CHAC1), POR, TFR, and Ptgs2 were largely up-regulated in the LPS/D-GalN group, while CHAC1 and TFR were down-regulated significantly in the DFOM+LPS/D-GalN group. There were no significant changes in POR and Ptgs2 between the LPS/D-GalN group and the DFOM+LPS/D-GalN group (Figure 5G-J). Moreover, DHODH, FSP1, XCT, and GPX4 were down-regulated in the LPS/D-GalN group while FSP1, GPX4, and XCT were up-regulated in the DFOM+LPS/D-GalN group, and DHODH showed no significant changes between them (Figure 5G-J).

In addition, we treated mice with ZVAD-FMK+Fer-1 to verify whether simultaneous inhibition of apoptosis and ferroptosis could relieve LPS/D-GalN-induced ALF. We recorded the survival rate and liver pathologic staining results of mice and found the simultaneous injection of ZVAD-FMK and Fer-1 could prolong the lifespan of mice compared with the LPS/D-GalN group (Figure 6A). Compared with the single-inhibitor group, H&E staining showed reduced cell swelling as well as diffuse intrahepatic hemorrhage and decreased hepatocyte death (Figure 6B).

In conclusion, we found that inhibition of apoptosis and ferroptosis could attenuate LPS/D-GalN-induced ALF by repressing caspase activation and inhibiting lipid peroxidation, improving the antioxidant capacity of the GSH/CoQ10 system and reducing iron accumulation.

ALF Induced by LPS/D-GalN Was Dependent on Macrophage-Derived TGF β

In the earlier-described study, we found that the macrophages in the liver increased significantly after LPS/D-GalN treatment (Figure 1E). Macrophages are a known source of TGF β ligands, particularly in the context of tissue injury.²¹ TGF β was expressed both by nonparenchymal cells and hepatocytes, in our study, we found that TGF β 1 secreted by macrophages was largely increased with LPS/D-GalN injection (Figure 7A). TGF β 1, the downstream receptor of TGF β 1, was expressed by hepatocytes in addition to nonepithelial cells.²¹ Therefore, we detected the expression of TGF β 1 in liver tissues and found that the protein expression of TGF β 1 was increased in liver tissues with LPS/D-GalN injection, as compared with the results in control mice (Figure 7B and C).

To address the role of TGF β 1 in LPS/D-GalN-induced ALF, we used B6.129-Alb^{tm1(CreERT2)Srcmo} and TGF β 1^{flox/flox} mice to construct tamoxifen-induced hepatic TGF β 1 deletion (TGF β 1^{Δhep-CKO}) mice, control mice also were derived from the homozygous offspring of B6.129-Alb^{tm1(CreERT2)Srcmo} and TGF β 1^{flox/flox} without tamoxifen induction,

abbreviated to TGF β 1^{Δhep} (Figure 7D). They were used to establish the LPS/D-GalN-induced ALF model. TGF β 1 expression was not observed in livers of TGF β 1^{Δhep-CKO} mice (Figure 7E). TGF β 1^{Δhep-CKO} mice turned out to be suppressed LPS/D-GalN-induced ALF as assessed by hepatic function parameters ALT and AST (Figure 7F). The histologic analysis also showed that liver congestion and reduced hepatocyte death were reduced in TGF β 1^{Δhep-CKO} mice, compared with TGF β 1^{Δhep} mice after LPS/D-GalN treatment (Figure 7G). Consistent with pathologic changes, the number of apoptotic cells also was decreased, while the number of proliferating cells was increased in TGF β 1^{Δhep-CKO} mice after LPS/D-GalN treatment as assessed by TUNEL and Ki67 immunofluorescence staining (Figure 7H). These results suggest that deletion of hepatic TGF β 1 improved liver regeneration and inhibited hepatocyte apoptosis. Moreover, we detected the apoptosis-related proteins and found the expression of BCL2 was increased while the expression of cleaved caspase 8 was decreased in TGF β 1^{Δhep-CKO} mice after LPS/D-GalN treatment (Figure 7I and J).

These findings suggest that the absence of liver TGF β 1 inhibited LPS/D-GalN-induced ALF by reducing hepatocyte apoptosis.

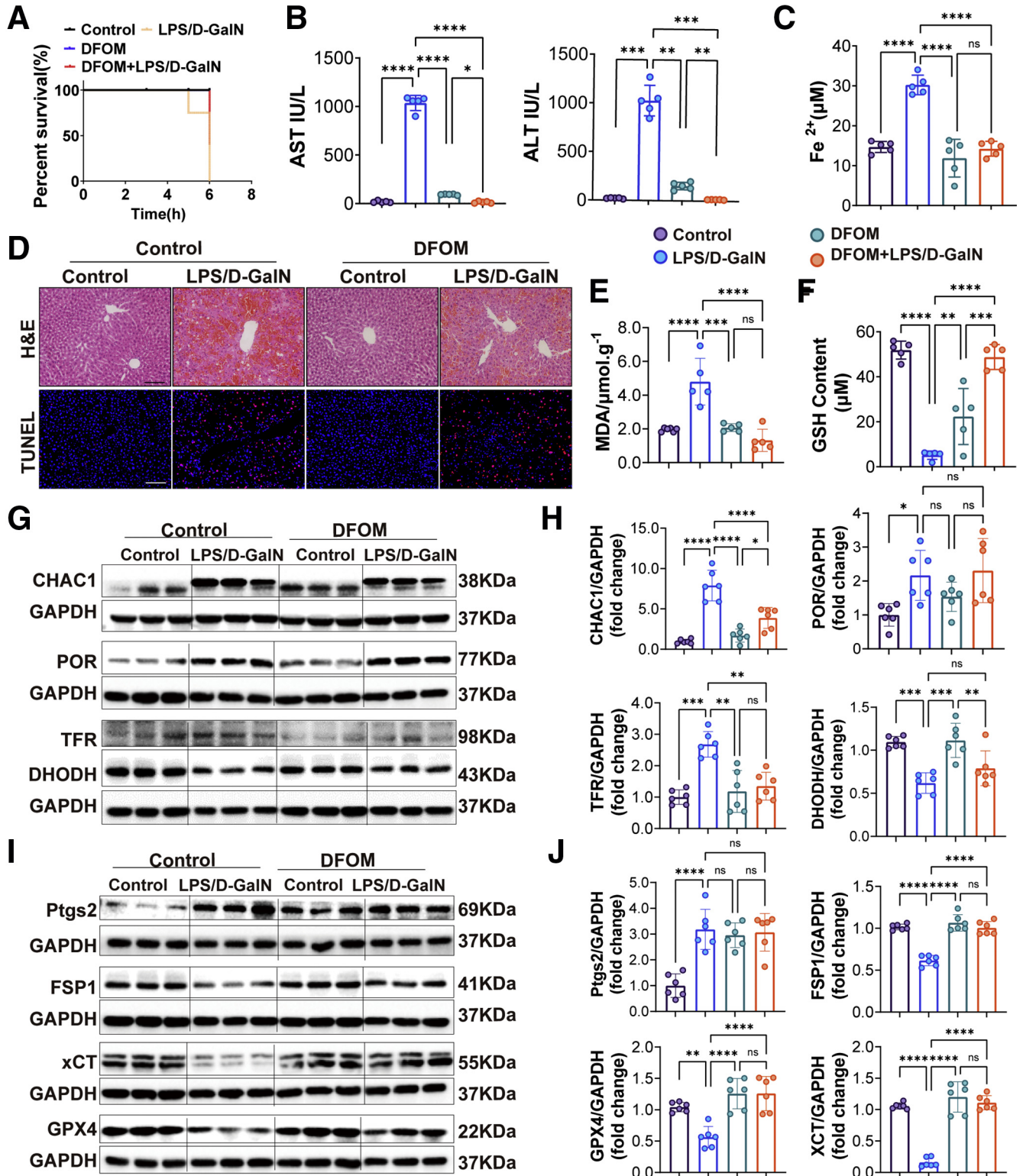
Deletion of Hepatic TGF β 1 Repressed ALF-Induced Ferroptosis and Reactive Nitrogen Species Accumulation

To characterize the role of TGF β 1 in ferroptosis, we evaluated the expression of several proteins involved in iron metabolism and lipid peroxidation in TGF β 1^{Δhep} mice and TGF β 1^{Δhep-CKO} mice co-injected with LPS/D-GalN. The expression of 4-HNE was reduced in TGF β 1^{Δhep-CKO} mice, although it was increased in TGF β 1^{Δhep} mice (Figure 8A and B). Then, we measured the level of lipid peroxidation in mice by MDA assay and found the level of MDA decreased in TGF β 1^{Δhep-CKO} mice treated with LPS/D-GalN (Figure 8D). We also detected the expression of CHAC1 and POR in mouse liver and found that the expression of CHAC1 was decreased in TGF β 1^{Δhep-CKO} mice treated with LPS/D-GalN. There were significant changes in POR expression between TGF β 1^{Δhep} and TGF β 1^{Δhep-CKO} mice (Figure 8I and J). These results indicate that TGF β 1 might play an important role in ferroptosis in regulating lipid peroxidation induced by LPS/D-GalN. Next, we detected an iron metabolism-related index. We found the level of Fe^{2+} was decreased in TGF β 1^{Δhep-CKO} mice treated with LPS/D-GalN (Figure 8C). The expression of TFR protein also was decreased in TGF β 1^{Δhep-CKO} mice (Figure 8G), which showed that TGF β 1 might play an important role in the process of iron metabolism.

Furthermore, we detected relevant indicators of anti-ferroptosis such as XCT/GPX4 and DHODH/FSP1. We found that the expression of both XCT and GPX4 protein were increased significantly in TGF β 1^{Δhep-CKO} mice (Figure 8E and G). Consistently, the expression of DHODH and FSP1 also were increased in TGF β 1^{Δhep-CKO} mice (Figure 8G and H). In addition, we detected the reactive nitrogen species

accumulation between TGFβ1^{Δhep} and TGFβ1^{Δhep-CKO} mice injected with LPS/D-GalN. We first measured the nitric oxide (NO) level of liver homogenate and found the increased NO level was reduced in TGFβ1^{Δhep-CKO} mice (Figure 9A). We also noticed the LPS/D-GalN-induced

inducible nitric oxide synthase (iNOS) increase was reduced in TGFβ1^{Δhep-CKO} mice. As shown in Figure 9B-G, in the LPS/D-GalN-treated group, both iNOS and nitro-tyrosine (NT) levels in TGFβ1^{Δhep-CKO} mice were lower than in TGFβ1^{Δhep} mice.



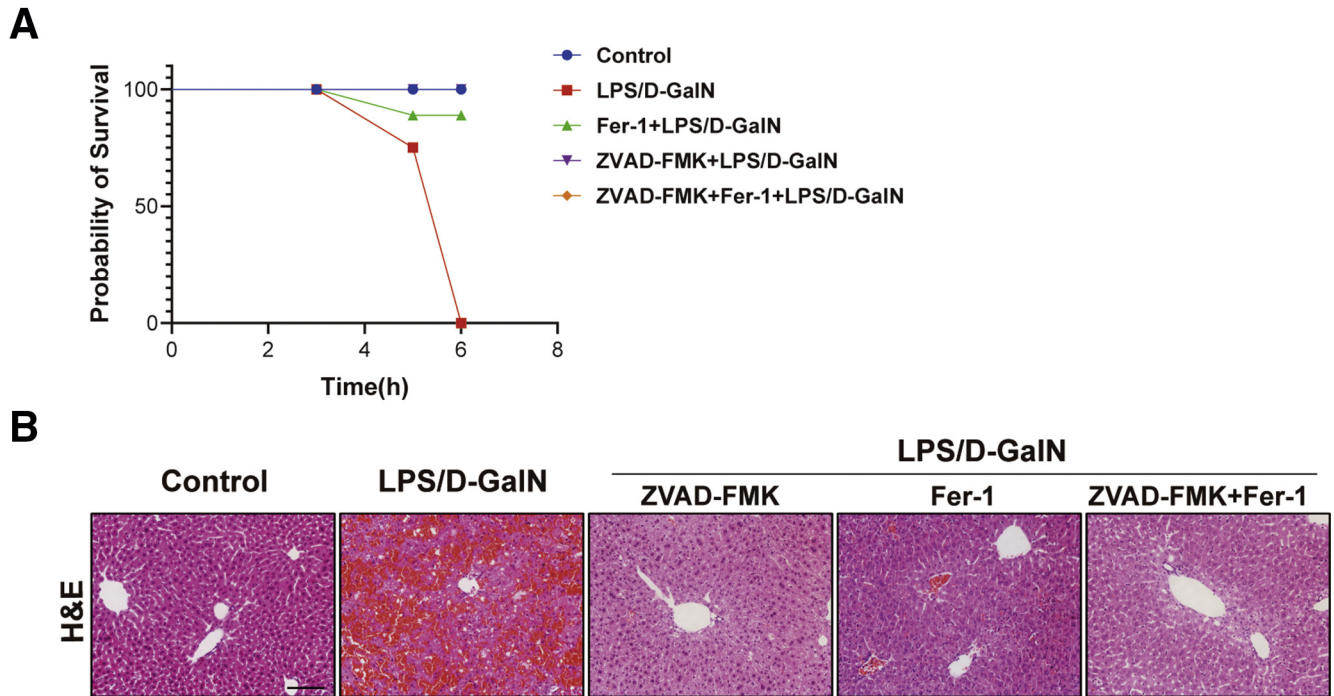


Figure 6. Simultaneous inhibition of ferroptosis and apoptosis alleviated LPS/D-GalN-induced ALF. (A) The survival rate of WT mice liver treated with ZVAD-FMK, Fer-1, or ZVAD-FMK+Fer-1 treatment before LPS/D-GalN co-injection ($n = 5$). (B) H&E staining of WT mouse liver treated with ZVAD-FMK, Fer-1, or ZVAD-FMK+Fer-1 treatment before LPS/D-GalN co-injection ($n = 5$). Scale bar: 50 μm . Data are presented as means \pm SEM. D-GalN, D-galactosamine.

The earlier-described data showed that $\text{TGF}\beta 1$ expression was crucial for the extent of ferroptosis and reactive nitrogen species accumulation induced by ALF.

TGF $\beta 1$ -Mediated LPS/D-GalN-Induced ALF Was Dependent on GSK3 β -Nrf2 Signaling

The earlier-described research provided evidence that $\text{TGF}\beta 1$ played critical roles in LPS/D-GalN-induced ALF, but the link between them is still not clear. A previous study elaborated that $\text{TGF}\beta 1$ remarkably abrogated the inhibitory phosphorylation of GSK3 β , potentially via activating protein phosphatase 1.¹⁷ Correspondingly, in our research, we performed double immunohistochemical staining of liver tissues with LPS/D-GalN treatment and found higher $\text{TGF}\beta 1$ (green) and GSK3 β (red) levels after LPS/D-GalN treatment (Figure 10A and B). Interestingly, GSK3 β is implicated in the hormonal control of several regulatory proteins including glycogen synthase. Under the electron microscope, we found that in mice with ALF, glycogen was reduced significantly

compared with the control group (Figure 10C and D). During the period of ALF, a large amount of secreted $\text{TGF}\beta 1$ promoted the expression of GSK3 β and decomposed a lot of glycogens in the liver, which is also the reason why patients with liver failure often have hypoglycemia, because the glycogen storage in the liver is reduced.

Recent evidence has suggested that GSK3 β is an inhibitory upstream component that regulates Nrf2 phosphorylation and subcellular P-GSK3 β , an anti-(phospho-Ser9)-GSK3 β -specific antibody that identifies GSK3 β in its Akt (known as protein kinase B)-phosphorylated inactive state.²⁶ Consistently, in our research, we found that with LPS/D-GalN treatment, both p-GSK3 β and Nrf2 were largely decreased in control mice, but rescued in $\text{TGF}\beta 1^{\Delta\text{hep-CKO}}$ mice (Figure 10E–I). In addition, we performed double immunohistochemical staining of liver tissues with LPS/D-GalN treatment and found higher Nrf2 (green) and p-GSK3 β (red) levels in $\text{TGF}\beta 1^{\Delta\text{hep-CKO}}$ mice compared with $\text{TGF}\beta 1^{\Delta\text{hep}}$ mice (Figure 10J). We also noticed that the

Figure 5. (See previous page). DFOM alleviated LPS/D-GalN-induced ALF by inhibiting ferroptosis. (A) The survival rate of WT mice treated with vehicle or DFOM (100 mg/kg) 1 hour before LPS/D-GalN co-injection ($n = 5$). (B) Serum levels of ALT and AST from WT mice with vehicle or DFOM before LPS/D-GalN co-injection ($n = 5$). (C) Serum of Fe^{2+} levels of WT mice with vehicle or DFOM before LPS/D-GalN co-injection ($n = 5$). (D) Representative pictures for H&E and TUNEL staining of WT mice with vehicle or DFOM before LPS/D-GalN co-injection ($n = 5$). (E and F) GSH and MDA assay of liver homogenates from WT mice with vehicle or DFOM before LPS/D-GalN treatment ($n = 5$). (G and H) Western blot analyses of CHAC1, POR, TFR, and Ptg2 from WT mice with vehicle or DFOM before LPS/D-GalN treatment and ratios of each protein to glyceraldehyde-3-phosphate dehydrogenase (GAPDH) ($n = 6$). (I and J) Western blot analyses of DHODH, FSP1, GPX4, and XCT from WT mice with vehicle or DFOM before LPS/D-GalN treatment and ratios of each protein to GAPDH ($n = 6$). All data were obtained from WT mice. Scale bars: 100 μm . Data are presented as means \pm SEM. * $P < 0.05$, ** $P < 0.01$, *** $P < 0.001$, **** $P < 0.0001$. D-GalN, D-galactosamine.

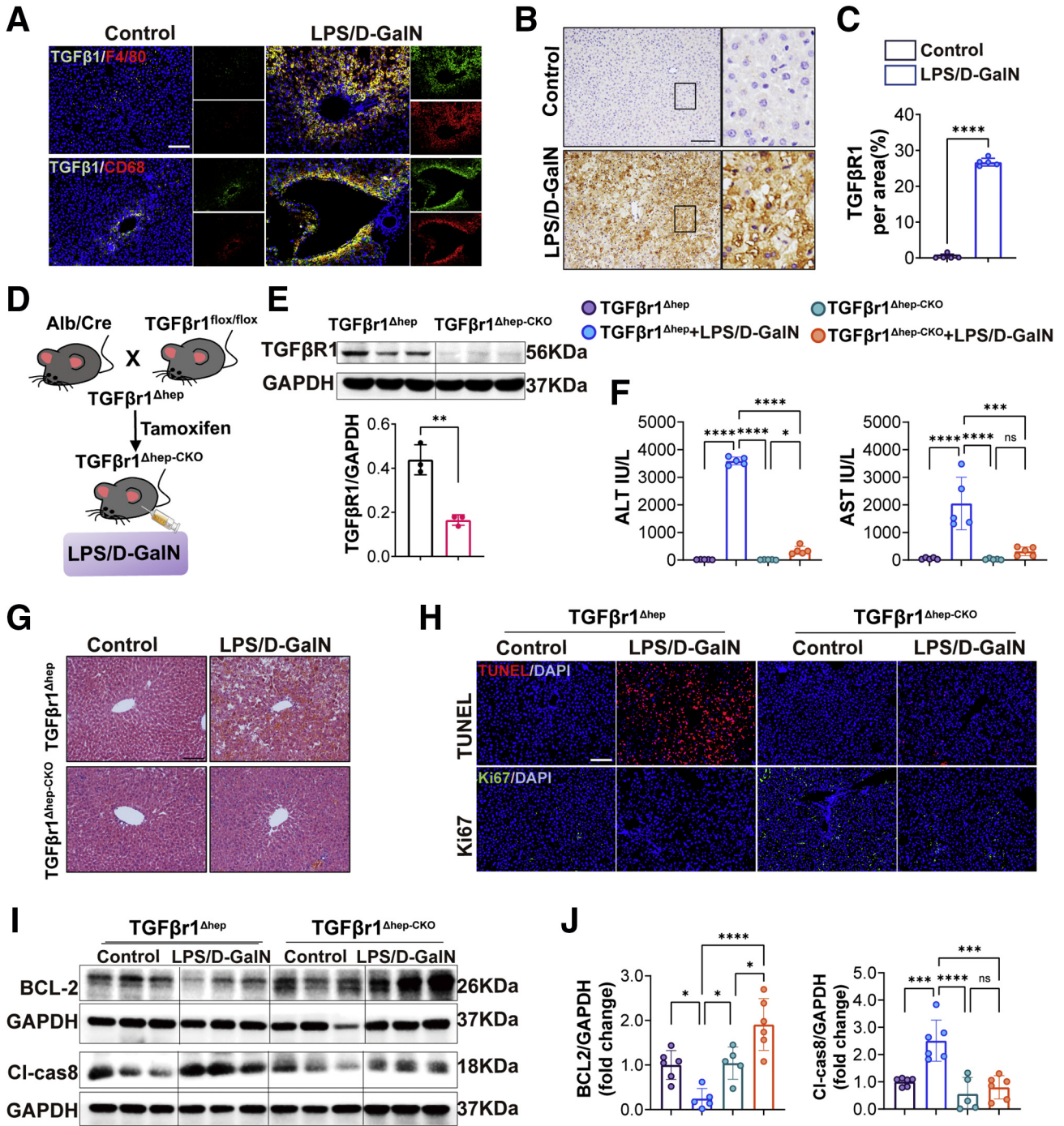


Figure 7. Hepatic TGFβ1 deletion inhibited LPS/D-GalN-induced ALF. (A) Immunofluorescence co-staining of TGFβ1/F480 and TGFβ1/CD68 from WT mice with or without LPS/D-GalN co-injection (n = 5). (B) Immunohistochemistry staining of TGFβ1 in livers and (C) quantitative results (n = 5). (D) Schematic protocol used for reproducing TGFβ1^{Δhep-CKO} mice. (E) Western blots of TGFβ1 in liver tissues and quantitative results of TGFβ1/GAPDH (n = 3). (F) Serum ALT and AST levels of TGFβ1^{Δhep-CKO} and TGFβ1^{Δhep} mice after vehicle or LPS/D-GalN treatment (n = 5). (G) H&E staining was performed on paraffin-embedded sections of mouse livers from TGFβ1^{Δhep-CKO} and TGFβ1^{Δhep} mice after vehicle or LPS/D-GalN treatment (n = 5). (H) Representative pictures for TUNEL assay and Ki67 immunofluorescence staining TGFβ1^{Δhep-CKO} and TGFβ1^{Δhep} mice after vehicle or LPS/D-GalN treatment (n = 5). (I) Western blot analyses of BCL2 and cl-caspase 8 proteins of TGFβ1^{Δhep-CKO} and TGFβ1^{Δhep} mice after vehicle or LPS/D-GalN treatment and their (J) ratios of each protein to GAPDH (n = 6). Scale bars: 100 μm; Data are presented as means ± SEM. *P < 0.05, **P < 0.01, ***P < 0.001, ****P < 0.0001. DAPI, 4',6-diamidino-2-phenylindole; D-GalN, D-galactosamine; GAPDH, glyceraldehyde-3-phosphate dehydrogenase.

expressions of p-GSK3 β and Nrf2 were reduced in TGF β 1 Δ hep mice while improved in TGF β 1 Δ hep-CKO mice after LPS/D-GalN co-injection. Considering that the increase in Nrf2 protein levels was correlated with the inactivation of

GSK3 β , we concluded that TGF β 1-mediated LPS/D-GalN-induced ALF was enhanced by promoting GSK3 β to inhibit Nrf2 expression, thereby inhibiting the body's antioxidant system.

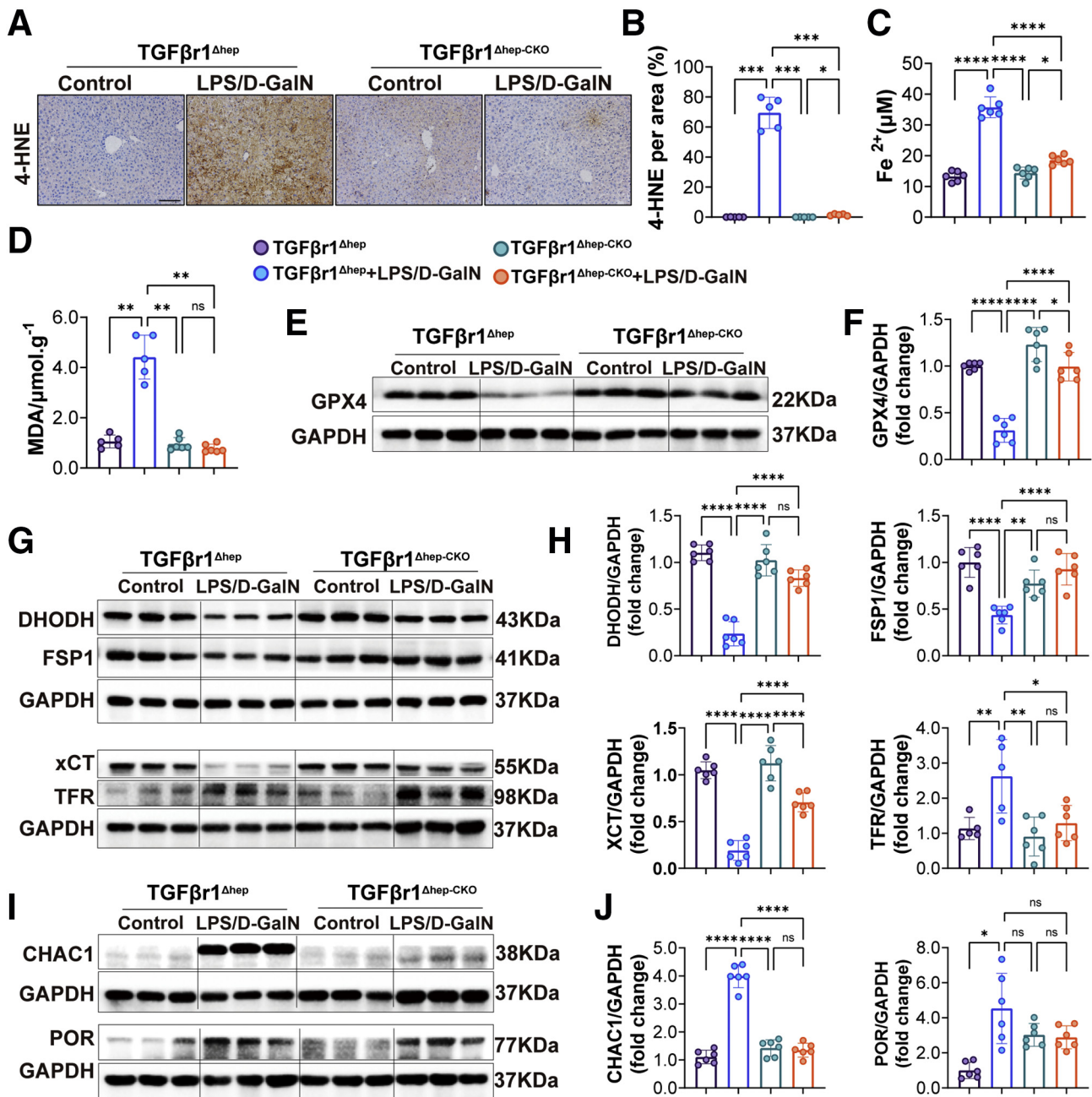


Figure 8. Hepatic TGF β 1 deletion repressed LPS/D-GalN-induced ferroptosis. (A and B) Immunohistochemistry staining of and 4-HNE in livers (right) of TGF β 1 Δ hep-CKO and TGF β 1 Δ hep mice after vehicle or LPS/D-GalN treatment and quantitative results (left). (C) Serum levels of Fe $^{2+}$ (n = 6) in TGF β 1 Δ hep-CKO and TGF β 1 Δ hep mice after LPS/D-GalN treatment. (D) MDA assay of liver homogenates from TGF β 1 Δ hep-CKO and TGF β 1 Δ hep mice after LPS/D-GalN treatment (n = 4). (E and F) Western blots of GPX4 expression in TGF β 1 Δ hep-CKO and TGF β 1 Δ hep mice liver and quantitative result of GPX4/GAPDH (n = 6). (G) Representative Western blots of DHODH, FSP1, xCT, GPX4, and TFR expression in TGF β 1 Δ hep-CKO and TGF β 1 Δ hep mice liver and (H) ratios of each protein to GAPDH (n = 6). (I) Representative western blots of CHAC1 and POR expression in TGF β 1 Δ hep-CKO and TGF β 1 Δ hep mice liver and (J) ratios of each protein to GAPDH (n = 6). All data are presented as means \pm SEM. Scale bar: 100 μ m. *P < 0.05, **P < 0.01, ***P < 0.001, ****P < 0.0001. D-GalN, D-galactosamine; GAPDH, glyceraldehyde-3-phosphate dehydrogenase.

Ferroptosis Was Enhanced by LPS/D-GalN-Induced ALF in Nrf2^{-/-}

Nrf2 is considered a master regulator of the antioxidant response because many of its downstream target genes are involved in preventing or correcting redox imbalances in the cell.²⁷ To further assess the role of Nrf2 in LPS/D-GalN-induced ALF, we performed ALT/AST and H&E staining of liver tissues in wild-type (WT) mice and Nrf2^{-/-} mice. Liver function and histologic examination showed more severe liver damage in Nrf2^{-/-} mice (Figure 11A and B). Furthermore, the relative values of oxidative stress markers (MDA, superoxide dismutase (SOD), and 4-HNE) were assessed. The percentage of MDA was increased significantly, while the percentage of SOD levels decreased significantly after LPS/D-GalN treatment. Compared with WT mice, MDA was increased in Nrf2^{-/-} mice (Figure 11C and D). Consistently, immunohistochemical staining showed 4-HNE was increased significantly in Nrf2^{-/-} mice (Figure 11B), indicating that Nrf2 played an important role in the body's antioxidant system. The expression of DMT1 was increased after LPS/D-GalN treatment and exacerbated in Nrf2^{-/-} mice (Figure 11E). In addition, examination of lipid peroxidation-related proteins (Ptgs2, CHAC1, and POR) (Figure 11E and I) indicated that ferroptosis was significantly greater in Nrf2^{-/-} mice than in WT mice because the expression of Ptgs2 was increased in Nrf2^{-/-} mice, when compared to WT mice. However, there were no significant differences in the expression of CHAC1 and POR. We further detected the expression of antioxidant system-related proteins (GPX4, XCT, FSP1, and DHODH) and found that the expression of GPX4 and FSP1 was decreased in Nrf2^{-/-} mice when compared to WT mice after LPS/D-GalN treatment (Figure 11G and H).

Subsequently, we conducted a rescue experiment on Nrf2^{-/-} mice to further assess the relationship between Nrf2 and LPS/D-GalN-induced ferroptosis. With Fer-1 treatment, the levels of serum AST and ALT were decreased drastically in Nrf2^{-/-} mice (Figure 12A). Histologic examination showed a normal liver structure and slight liver congestion in Nrf2^{-/-} mice after Fer-1 treatment (Figure 12B). The percentage of MDA level was decreased while the percentage of SOD level was increased significantly in Nrf2^{-/-} mice with Fer-1 injection (Figure 12C and D). The expression of 4-HNE, Ptgs2, and DMT1 proteins also was decreased significantly in Nrf2^{-/-} mice after Fer-1 treatment (Figure 12F–I). At the same time, inflammatory cell infiltration in the liver also was reduced in Nrf2^{-/-} mice with Fer-1 injection (Figure 12E).

Therefore, these results suggest that ferroptosis was more severe in Nrf2^{-/-} mice compared with WT mice, and Fer-1 protected Nrf2^{-/-} mice from ferroptosis induced by LPS/D-GalN.

Nrf2 Was Essential for the Hepatoprotective Effect of Hepatic TGF β 1 Knockout

The earlier-described experiments indicated that Nrf2 played an important role in LPS/D-GalN-induced ALF by

inhibiting ferroptosis. To further confirm the protective effect of liver TGF β 1 knockout in LPS/D-GalN-induced ALF was owing to Nrf2, we constructed the adeno-associated virus serotype 9 (AAV9)-NFE2 like bZIP transcription factor 2 (Nfe2l2)-RNA interference (RNAi) virus-carrying flanked by loxp (flox) tags to perform the following experiment. The AAV9-Nfe2l2-RNAi virus was injected through the tail vein, and the injection volume was 2×10^{11} vg (unit of virus titer) per mouse through pre-experimental testing. As shown in Figure 13, 7 days after being injected with tamoxifen to induce TGF β 1 ^{Δ hep-CKO}, these mice were respectively treated with AAV9-Nfe2l2-RNAi (Nrf2-RNAi) and negative control (NC) virus, by tail vein injection.

As the H&E and liver function tests show, after LPS/D-GalN treatment, mice in the Nrf2-AAV group showed more severe destruction of liver structure, diffuse hemorrhagic necrosis, and hepatocyte apoptosis than the NC group because there was spotted sheet cell death in the liver, as well as increased ALT and AST levels (Figure 13A and B). However, compared with the previous results in Nrf2^{-/-} ALF mice (Figure 11), liver cell death was reduced, liver function ALT and AST was reduced in Nrf2-RNAi+TGF β 1 ^{Δ hep-CKO} mice, which indicated TGF β 1 has inhibitory effects on Nrf2 during ALF. Moreover, we found that the level of MDA was increased significantly in the Nrf2-RNAi+TGF β 1 ^{Δ hep-CKO} mice compared with the NC+TGF β 1 ^{Δ hep-CKO} group (Figure 13C). We also detected ferroptosis-related protein and found that DHODH, FSP1, GPX4, and XCT were decreased significantly while TFR was increased in the Nrf2-RNAi+TGF β 1 ^{Δ hep-CKO} mice compared with the NC+TGF β 1 ^{Δ hep-CKO} group. However, the expression of Ptgs2 and POR did not change significantly in the NC and Nrf2-RNAi groups (Figure 13D–G).

Taken together, combined with the results in Figure 11, we have reason to believe that TGF β 1 is involved in ferroptosis in the process of ALF by regulating the Nrf2-mediated antioxidant system. Nrf2 was especially essential for the protective effect of hepatic TGF β 1 knockout in ALF.

Discussion

ALF is a rare clinical disease with high morbidity and mortality, the most effective treatment at present is liver transplantation.²⁸ Although hepatocyte cell death is considered to be the critical event in ALF, the underlying mechanism remains unclear. ALF is characterized by massive loss of parenchymal cells, including the release of cell contents, cell swelling, and inflammation, commonly used experimental models related to ALF are the APAP-based and LPS/D-GalN-based models. In APAP-induced ALF, APAP enters the body and is converted by cytochrome P450 enzymes to the toxic metabolite N-acetyl-p-benzoquinone, which immediately binds to GSH for detoxification. However, when APAP is overtaken, GSH is depleted by excess N-acetyl-p-benzoquinone and leads to oxidative stress and hepatocyte necrosis.²⁹ Hepatocyte necrosis generally is considered to be the predominant type of cell death in APAP-induced ALF.³⁰ However, there are also

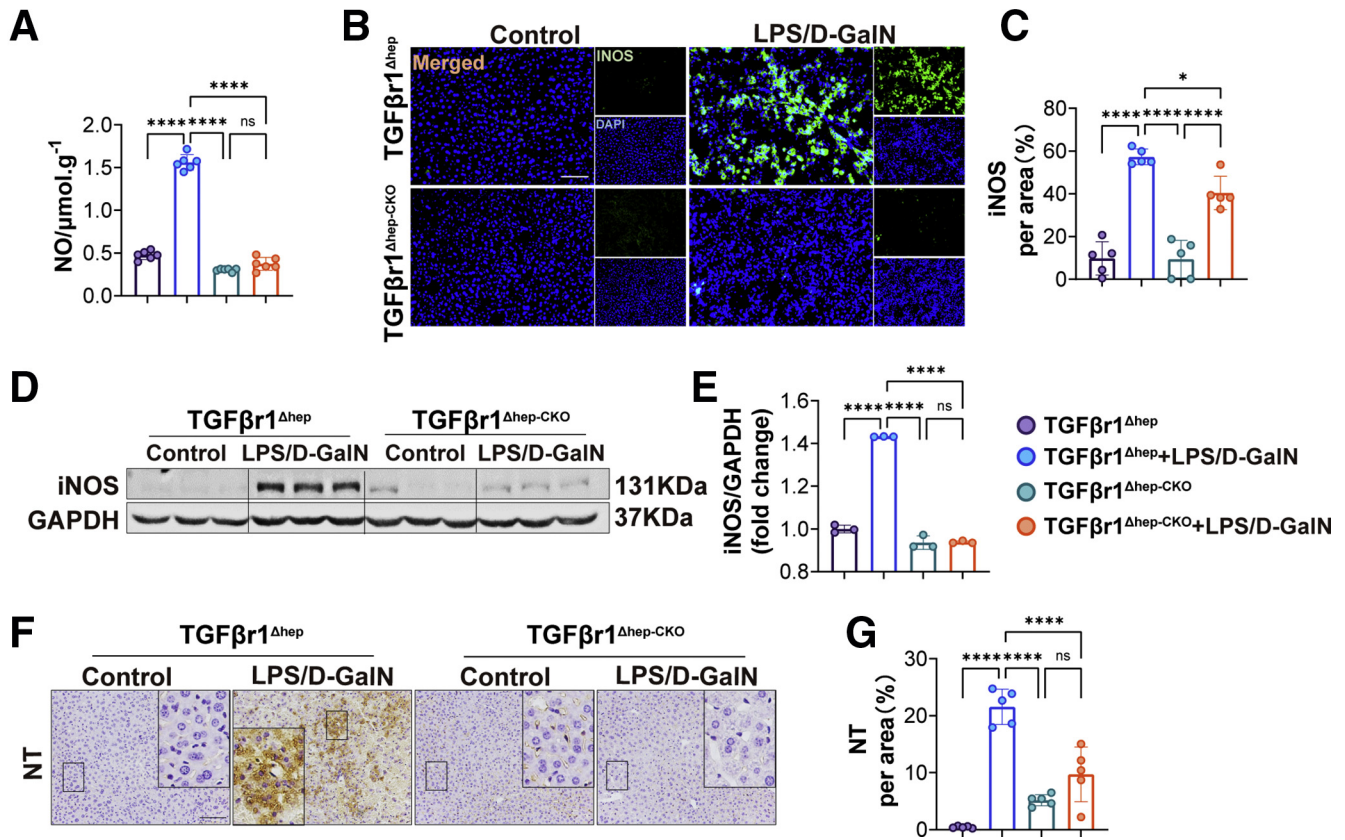


Figure 9. Hepatic TGFβ1 deletion repressed LPS/D-GaIN-induced reactive nitrogen species accumulation. (A) NO level of TGFβ1^{Δhep-CKO} and TGFβ1^{Δhep} mice after vehicle or LPS/D-GaIN treatment (n = 6). (B) Representative pictures for iNOS immunofluorescence staining and (C) quantitative results (n = 5). (D and E) Western blot assay of iNOS from TGFβ1^{Δhep-CKO} and TGFβ1^{Δhep} mice after vehicle or LPS/D-GaIN treatment and result of iNOS/GAPDH (n = 3). (F) Immunohistochemistry staining of NT and (G) quantitative results (n = 5). Data are presented as means ± SEM. *P < 0.05, **P < 0.01, ***P < 0.001, ****P < 0.0001. Scale bars: 50 μm. DAPI, 4',6-diamidino-2-phenylindole; D-GaIN, D-galactosamine; GAPDH, glyceraldehyde-3-phosphate dehydrogenase.

more and more studies showing that ferroptosis plays an important role in APAP-induced ALF.^{15,31–33} As Jaeschke et al³⁴ said, if we are going down a rabbit hole, as ferroptosis occurs not only requires a large amount of lipid peroxide (LPO) but also requires complex processes such as accumulation of iron, peroxidation of PUFAs in cell membranes. Evidence that an APAP overdose causes ferroptosis cell death is still lacking. In LPS/D-GaIN-induced ALF, pathophysiology begins with the binding of LPS to Toll-like receptor 4 on Kupffer cells, which triggers TNFα-induced apoptosis.^{23,35,36} Previous research has shown that inflammatory responses, oxidative stress, endoplasmic reticulum (ER) stress, and apoptosis mainly contributed to LPS/D-GaIN-induced ALF.^{30,37–40} However, Liu et al⁴¹ and Yang et al⁴² found that pyroptosis occurred in LPS/D-GaIN-induced ALF through activating caspase 1 and inflammasome NLR family pyrin domain containing 3 (NLRP3). Studies also showed that ferroptosis took place in LPS/D-GaIN-induced ALF by increasing lipid peroxidation with cyclooxygenase (COX) and lysyl oxidase (LOX) pathway up-regulation and inhibiting GSH synthesis.^{43–46} Whether

ferroptosis occurs during LPS/D-GaIN-induced ALF is still controversial and more adequate and detailed experimental data are urgently needed. In our study, we provided evidence that ferroptosis existed in LPS/D-GaIN-induced ALF from a more careful and comprehensive characterization of ferroptosis features. With electron microscopy, we found that mitochondria in the LPS/D-GaIN group appeared smaller than in the control group, with increased membrane density. Because ferroptosis is characterized by the overwhelming, iron-dependent accumulation of lethal lipid ROS,⁹ we separately examined iron metabolism and lipid ROS. Excessive Fe²⁺ can cause a Fenton reaction, resulting in a large amount of ROS, and we found the expression of TFR and DMT1 were increased and the levels of Fe²⁺ also were increased during LPS/D-GaIN-induced ALF. In addition, we also detected the related proteins of the GSH and CoQ10 antioxidant system and found that GPX4/XCT and FSP1/DHODH were decreased significantly during LPS/D-GaIN-induced ALF. Furthermore, we detected lipid peroxidation-related proteins such as Ptgs2 and POR and found they were largely increased in LPS/D-GaIN-induced ALF. Notably,

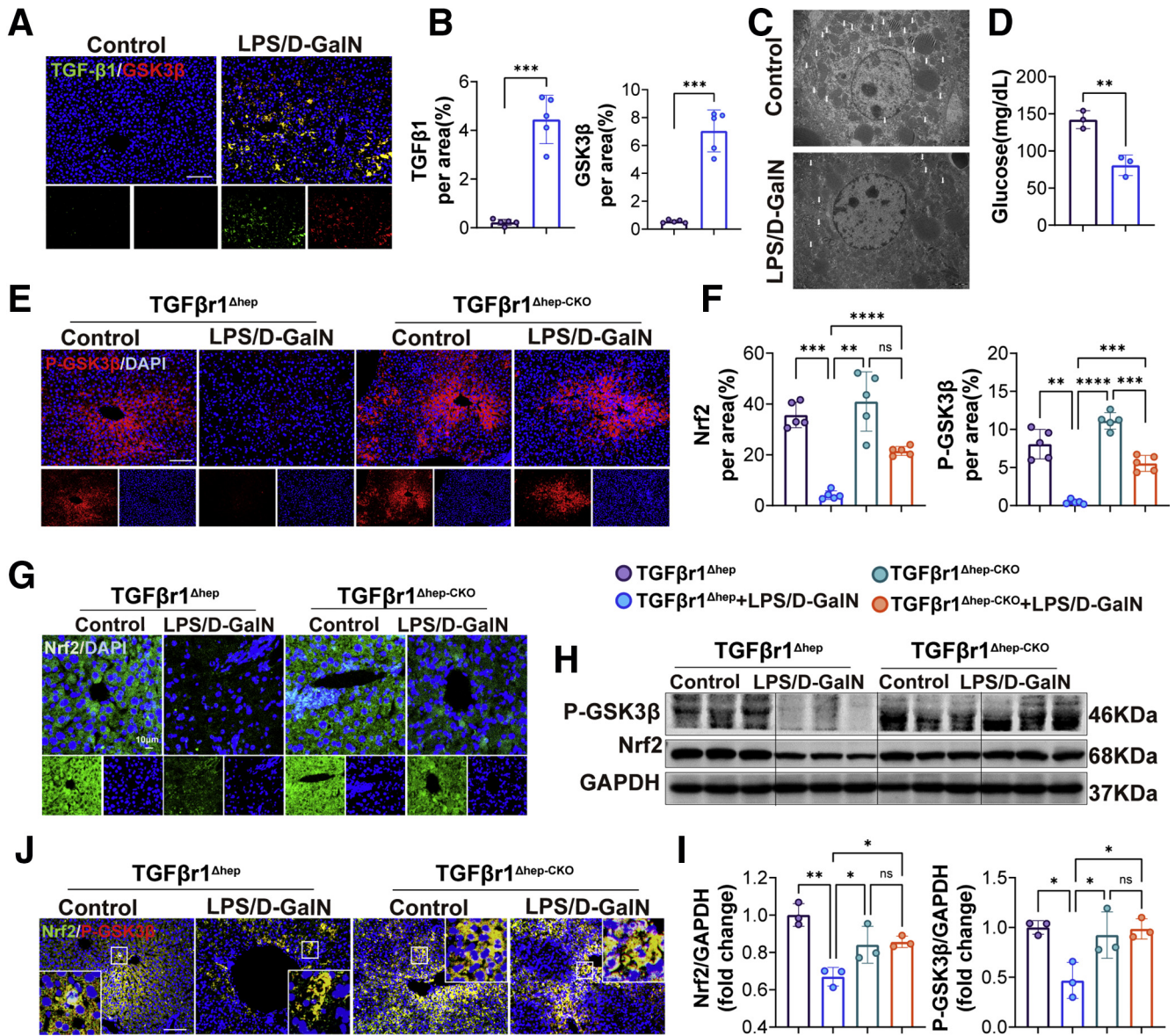


Figure 10. $TGF\beta 1$ -mediated LPS/D-GalN-induced ALF was dependent on GSK-3 β /Nrf2 signaling. (A) Immunofluorescence co-staining of $TGF\beta 1$ and GSK3 β from WT mice treated with vehicle or LPS/D-GalN and (B) quantitative assay ($n = 5$). Scale bars: 100 μm . (C) Electron microscopy of liver tissues from WT mice treated with vehicle or LPS/D-GalN. (D) Glucose assay of mice serum treated with vehicle or LPS/D-GalN ($n = 3$). (E) Representative pictures for p-GSK3 β from $TGF\beta 1^{\Delta\text{hep-CKO}}$ and $TGF\beta 1^{\Delta\text{hep}}$ mice after vehicle or LPS/D-GalN treatment and (F) quantitative results ($n = 5$). Scale bars: 100 μm . (G) Nrf2 immunofluorescence staining of $TGF\beta 1^{\Delta\text{hep-CKO}}$ and $TGF\beta 1^{\Delta\text{hep}}$ mice after vehicle or LPS/D-GalN treatment ($n = 5$). Scale bars: 10 μm . (H) Representative Western blots of p-GSK3 β , Nrf2 from $TGF\beta 1^{\Delta\text{hep-CKO}}$ and $TGF\beta 1^{\Delta\text{hep}}$ mice after vehicle or LPS/D-GalN treatment and (I) ratios of each protein to GAPDH ($n = 3$). (J) Immunofluorescence co-staining of p-GSK3 β (red) and Nrf2 (green) from $TGF\beta 1^{\Delta\text{hep-CKO}}$ and $TGF\beta 1^{\Delta\text{hep}}$ mice after vehicle or LPS/D-GalN treatment. Scale bars: 100 μm . All data are presented as means \pm SEM. * $P < 0.05$, ** $P < 0.01$, *** $P < 0.001$, **** $P < 0.0001$. DAPI, 4',6-diamidino-2-phenylindole; D-GalN, D-galactosamine; GAPDH, glyceraldehyde-3-phosphate dehydrogenase.

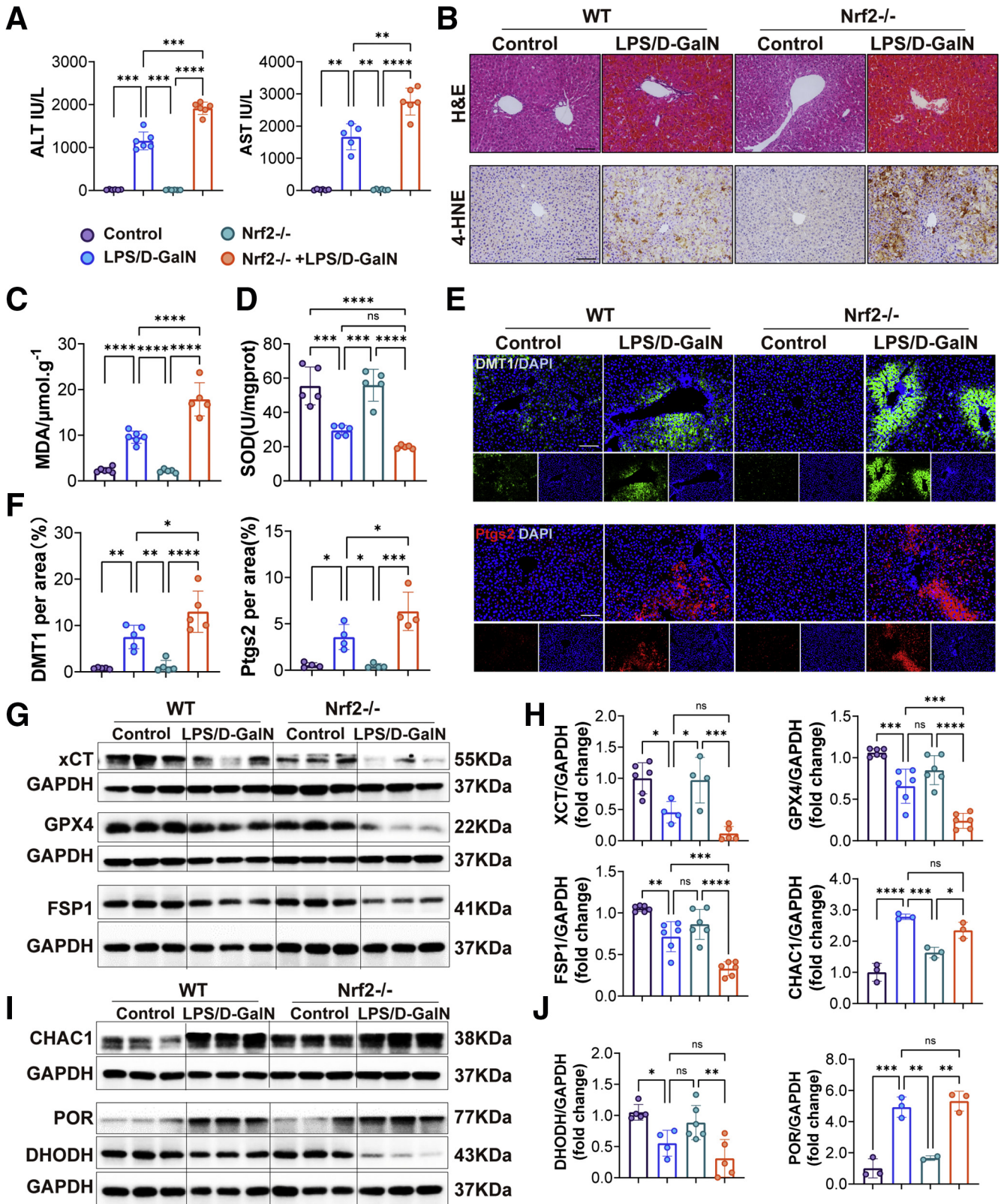
in reverse validation experiments, we found that Fer-1 and DFOM could prolong the mouse survival rate and alleviate liver injury.

It is worth mentioning that during our experiments we found the level of NO was increased in the LPS/D-GalN group and decreased in the control group, similar results also appeared in the expression levels of iNOS and NT. A recent study⁴⁷ showed that iNOS could induce a mixture of

apoptosis, necroptosis, and pyroptosis, so we detected the expression of receptor-interacting protein kinase 3 (RIP3) and gasdermin D (GSDMD). Unfortunately, we found no significant changes in RIP3 and GSDMD (Figure 2D and E). At the same time, we also established an in vitro model of hepatocyte-L02 injury model by using LPS/D-GalN (LPS, 10 ng/mL; D-GalN, 1 mmol/L) according to former research.⁴⁸ By using inhibitors such as Fer-1 (ferroptosis inhibitor),

ZVAD-FMK (apoptosis inhibitor), and necrostatin-1 (Nec-1, RIP1 inhibitor), we found that Fer-1 and ZVAD-FMK could promote L02 proliferation after LPS/D-GalN treatment

while Nec-1 could not (Figure 2F and G). In a previous study, apoptosis-related caspase proteins were activated such as caspase 3, but the activity of caspase 1 (interleukin



1 β -converting enzyme)-like proteases did not change during LPS/D-GalN-induced ALF.²³ In addition, another study also showed that nitroxide stress was involved in the process of ferroptosis.⁷ Combined with our experimental data, we believe that a large number of free radicals are generated during nitroxide stress to promote ferroptosis. However, there is no sufficient evidence to conclude that necrosis and pyroptosis occur in LPS/D-GalN-induced ALF. More in-depth research is needed.

Excessive ROS are produced in liver cells during ALF, which leads to oxidative stress. Upon oxidative stress, mammalian cells immediately will initiate a highly efficient cytoprotective machinery to protect cells against the harmful effects of ROS. The study also showed that in LPS/D-GalN-induced ALF, TNF α triggers early cell death and the recruited neutrophils generated ROS.⁴⁹ Similarly, in our experiments we found that TNF α was increased, accompanied by the increase in the expression of LY6G, indicating that TNF α recruited neutrophils and generated excessive ROS in the early stage of ALF. The Nrf2 antioxidant response pathway, the primary cellular defense signaling against the cytotoxic effects of oxidative stress, is essential for ALF.⁵⁰ Thus, GSK3 β now is recognized as a central regulator of cellular events. Emerging research has confirmed that GSK3 β is activated in the progression of ALF, and GSK3 β inhibition can ameliorate hepatotoxicity in ALF mice.^{51,52} In the past few decades, the role of GSK3 β in ALF has been attributed to the regulation of Nrf2 oxidative stress.⁵³ GSK3 β functions as an inhibitor, both directly in the activation and indirectly in the postinduction of Nrf2.^{54,55} Consistently, in our study, we found that the expression of GSK3 β was largely increased, which was consistent with the expression of TGF β 1, while Nrf2 was decreased significantly in LPS/D-GalN-induced ALF. Moreover, ferroptosis was exacerbated in Nrf2^{-/-} mice with LPS/D-GalN treatment, the expression of DHODH, FSP1, GPX4, and XCT were decreased significantly while TFR was increased in the Nrf2-RNAi+TGF β 1^{Δ_{hep-CKO}} mice compared with the NC group in LPS/D-GalN-induced ALF, indicating that GSK3 β -Nrf2 plays an important role in regulating ferroptosis in ALF, and Nrf2 is essential for the protective effect of hepatic TGF β 1 knockout in ALF.

Mechanistically, deletion of hepatic TGF β 1 was found in the present study to be effective for alleviating ALF. Our finding was in agreement with previous studies, the plasma levels and hepatic messenger RNA expression of TGF β 1 were increased significantly in patients with fulminant hepatic failure.^{19,20,56} In another study conducted by

Thomas et al.,²¹ TGF β 1 inhibition reduced senescence and enhanced liver regeneration for treating APAP poisoning. Taken together, the current research indicates that TGF β 1 plays an important role in ALF and aggravates liver failure by inhibiting liver regeneration. In our research, however, deletion of hepatic TGF β 1 was found to be sufficient and essential for GSK3 β -Nrf2 to exert an anti-oxidant response in ferroptosis induced by ALF. In a former study performed by Michaeloudes et al.,⁵⁷ TGF β 1 triggered intracellular ROS release in airway smooth muscle cells by up-regulation of nicotinamide adenine dinucleotide phosphate (NADPH) oxidase 4 and inhibited Nrf2-antioxidant response in cultured airway smooth muscle cells. In addition, with the presence of TGF β 1, the cytoprotective Nrf2 response was drastically impaired by GSK3 β in hepatitis C virus.¹⁷ Consistent with the role of GSK3 β in controlling the Nrf2 reaction, TGF β 1 may significantly abolish the inhibitory phosphorylation of GSK3 β by activating protein phosphatase 1, because tautomycin, a specific inhibitor of protein phosphatase 1, has an inhibitory effect on TGF β 1. TGF β 1 has been confirmed to activate protein phosphatase 1,⁵⁸ which is highly involved in the dephosphorylation of serine 9 residue GSK3 β .⁵⁹ Therefore, it is conceivable that TGF β 1 induces the dephosphorylation of GSK3 β and reduces the inhibitory phosphorylation of GSK3 β by activating protein phosphatase 1, thereby enhancing the activity of GSK3 β , amplifying the phosphorylation of GSK3 β substrates (such as Nrf2), and ultimately promoting nuclear exit and degradation of Nrf2 and diminishing the Nrf2 response.

Generally, our experimental results provide a new perspective to re-understand ALF. We provide laboratory evidence that ferroptosis is present in ALF and show that TGF β 1 plays an important role in LPS/D-GalN-induced ALF through GSK3 β -Nrf2-mediated hepatocyte apoptosis and ferroptosis. However, our study does not address whether TGF β 1 or ferroptosis inhibitor is effective for acute liver injury and failure in human beings, and further human safety and efficacy studies are required. Moreover, there is no further in vitro experiment on the effect of TGF β 1 and ferroptosis on ALF.

Materials and Methods

Experimental Animals and Ethics Statement

Male C57BL/6 WT, Nrf2^{-/-} (strain Nrf2tm1Ywk/J), B6.129-Alb^{tm1(CreERT2)Srcmo}, TGF β 1^{flox/flox} (Jackson Laboratory, Bar Harbor, ME) mice between 9 and 12 weeks of age

Figure 11. (See previous page). Ferroptosis was enhanced by LPS/D-galactosamine (D-GalN)-induced ALF in Nrf2^{-/-} mice compared with WT mice. (A) Serum ALT and AST levels of WT and Nrf2^{-/-} mice treated with vehicle or LPS/D-GalN (n = 6). (B) H&E staining and 4-HNE immunohistochemistry staining of WT mice and Nrf2^{-/-} mice with or without LPS/D-GalN co-injection (n = 6). (C and D) MDA and SOD assay of WT mice and Nrf2^{-/-} mice with or without LPS/D-GalN co-injection (n = 6). (E) Representative pictures for DMT1 (green) and Ptgs2 (red) immunofluorescence staining from WT and Nrf2^{-/-} mice treated with or without LPS/D-GalN and (F) quantitative results (n = 4–5). (G) Representative Western blots of XCT, GPX4, FSP1, and DHODH from WT and Nrf2^{-/-} mice treated with or without LPS/D-GalN and (H) ratios of each protein to GAPDH. (I) Representative Western blots of CHAC1 and POR from WT and Nrf2^{-/-} mice treated with or without LPS/D-GalN and (J) ratios of each protein to GAPDH (n = 3). All data are presented as means \pm SEM. *P < 0.05, **P < 0.01, ***P < 0.001, ****P < 0.0001. Scale bar: 100 μ m. DAPI, 4',6-diamidino-2-phenylindole; D-GalN, D-galactosamine; GAPDH, glyceraldehyde-3-phosphate dehydrogenase.

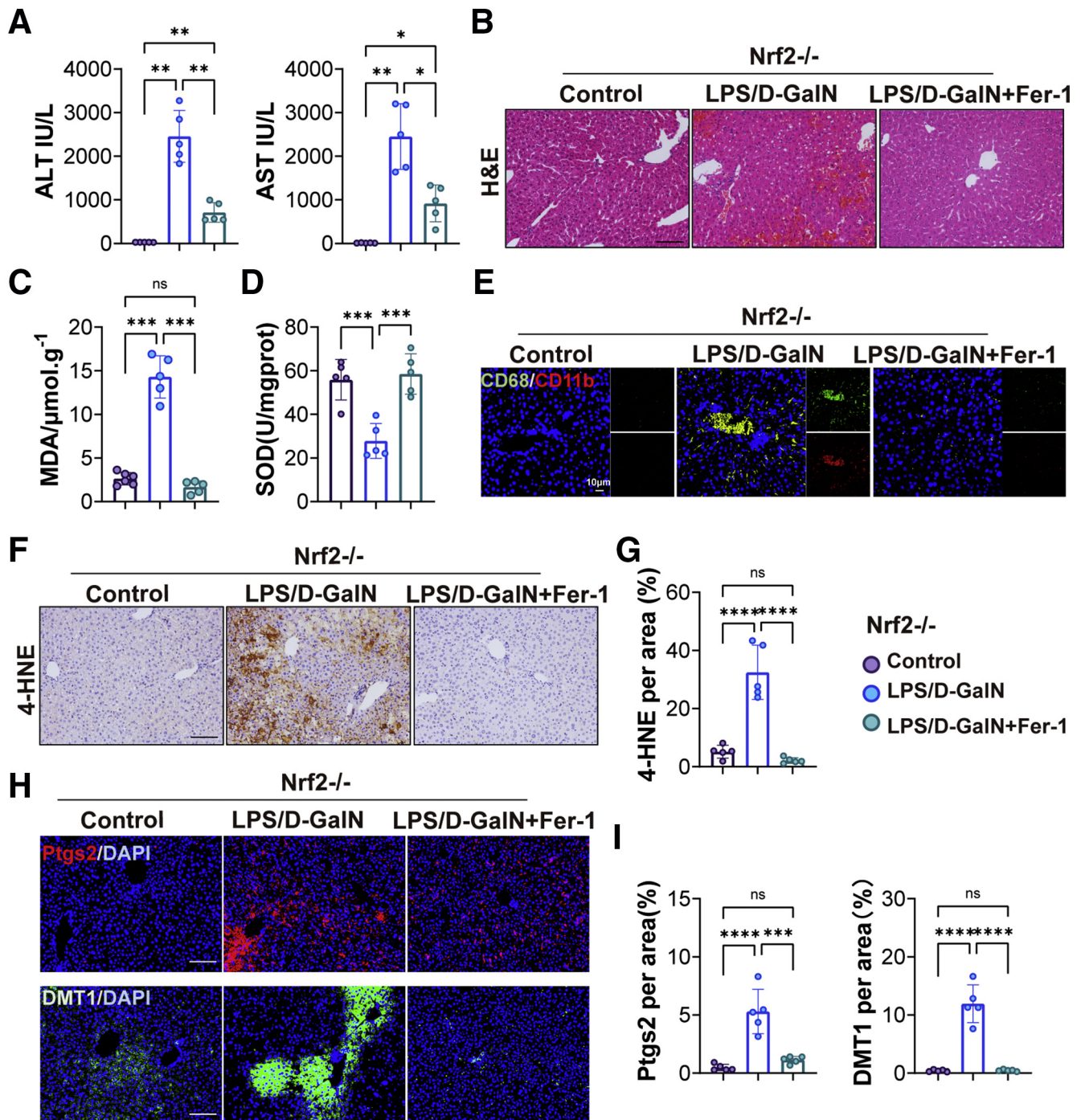


Figure 12. Fer-1 protected *Nrf2*^{-/-} mice from ferroptosis induced by LPS/D-GaIN. (A) Serum levels of ALT and AST of *Nrf2*^{-/-} mice with or without Fer-1 treatment (n = 5). (B) H&E staining of *Nrf2*^{-/-} mice with or without Fer-1 treatment (n = 5). Scale bars: 100 μm. (C) MDA and (D) SOD assay of *Nrf2*^{-/-} mice with or without Fer-1 treatment (n = 5). (E) Immunofluorescence co-staining of CD11b (red) and CD68 (green) from *Nrf2*^{-/-} mice with or without Fer-1 treatment (n = 5). Scale bars: 10 μm. (F) Immunohistochemistry staining of 4-HNE in livers from *Nrf2*^{-/-} mice with or without Fer-1 treatment and (G) quantitative results (n = 5). (H) Representative pictures for DMT1 (green) and Ptgs2 (red) immunofluorescence staining from *Nrf2*^{-/-} mice with or without Fer-1 treatment and (I) quantitative results (n = 5). Scale bars: 100 μm. All data are presented as means ± SEM. **P* < 0.05, ***P* < 0.01, ****P* < 0.001, *****P* < 0.0001. DAPI, 4',6-diamidino-2-phenylindole; D-GaIN, D-galactosamine.

were genotyped, housed under specific pathogen-free conditions. Tamoxifen-induced, hepatic-specific conditional *TGFβ1* knock-out mice were generated by *TGFβ1*^{fl^{ox}/fl^{ox}}

and *B6.129-Alb^{tm1(CreERT2)Srcmo}* mice. Tamoxifen (20 mg/mL) was administered via intraperitoneal injection once every 24 hours for a total of 5 consecutive days to induce

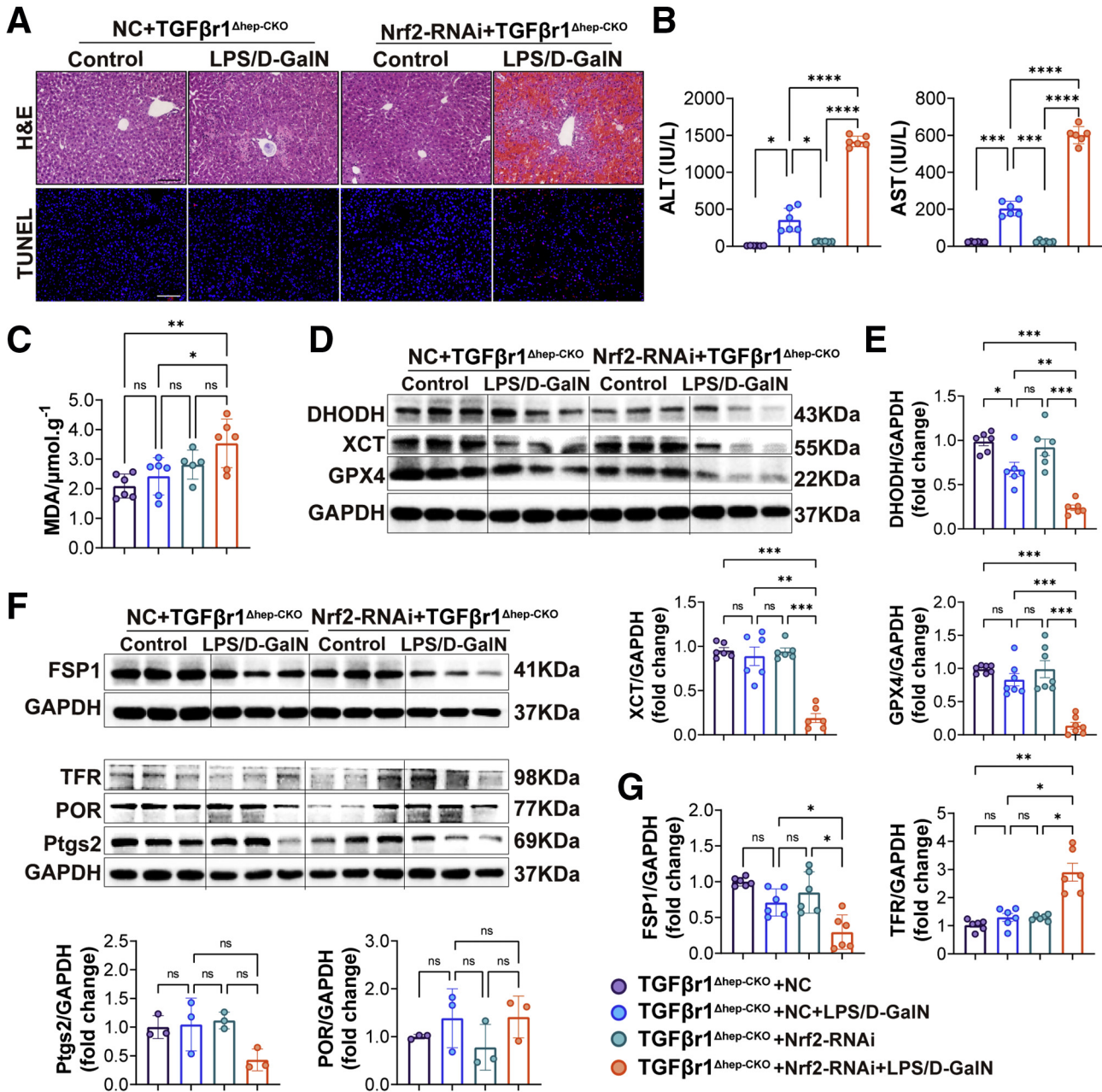


Figure 13. Nrf2 was essential for the protective effect of hepatic TGF β 1 knockout in ALF. (A) Representative pictures for H&E and TUNEL staining of TGF β 1 Δ hep-CKO mice tail vein injected with AAV9-NC or AAV9-Nrf2-RNAi virus (2×10^{11} vg/per mouse) 3 weeks before LPS/D-GalN co-injection ($n = 6$). (B) Serum levels of ALT and AST of TGF β 1 Δ hep-CKO mice carrying AAV9-NC or AAV9-Nrf2-RNAi virus with LPS/D-GalN treatment ($n = 6$). (C) MDA assay of TGF β 1 Δ hep-CKO mice carrying AAV9-NC or AAV9-Nrf2-RNAi virus with or without LPS/D-GalN treatment ($n = 6$). (D) DHODH, XCT, and GPX4 Western blot analyses of TGF β 1 Δ hep-CKO mice carrying AAV9-NC or AAV9-Nrf2-RNAi virus with or without LPS/D-GalN treatment and (E) ratios of each protein to GAPDH ($n = 6$). (F and G) FSP1, TFR, POR, and Ptgs2 Western blot analyses of TGF β 1 Δ hep-CKO mice carrying AAV9-NC or AAV9-Nrf2-RNAi virus with or without LPS/D-GalN treatment (F) and ratios of each protein to GAPDH (G) ($n = 3-6$). All data are presented as means \pm SEM. * $P < 0.05$, ** $P < 0.01$, *** $P < 0.001$, **** $P < 0.0001$. Scale bars: 100 μ m. GAPDH, glyceraldehyde-3-phosphate dehydrogenase.

hepatic-specific conditional TGF β 1 knock-out mice (TGF β 1 Δ hep-CKO).

The murine model of ALF was characterized previously. Adult male mice weighing 20–22 g were injected intraperitoneally with LPS (20 μ g/kg, *Escherichia coli*, L2630; Sigma,

Saint Louis, MO) in 100 μ L saline 15 minutes before injection of D-GalN (700 mg/kg, G0500; Sigma, Saint Louis, MO) in 100 μ L saline. Mice were killed 6 hours after LPS and D-GalN administration. ZVAD-FMK (S7023), DFOM (S5742), and Fer-1 (S7243) inhibitors were purchased from Selleck

(Houston, TX). All the procedures used in the animal studies were approved by the National Institutional Animal Care and Ethical Committee of Southern Medical University. All the experimental methods performed in this study were by the approved guidelines.

Histologic Analysis

Liver tissues were fixed in 4% paraformaldehyde overnight at 4°C, dehydrated, soaked in xylene, and embedded in paraffin in sequence, and then sliced into 4- μ m sections. Paraffin sections were dewaxed with xylene, dehydrated with different concentrations of ethanol, stained with H&E, dehydrated, cleared, sealed, and finally imaged under a light microscope (Eclipse Ni-U; Nikon, Tokyo, Japan).

Base Biochemical Parameters

Serum was acquired by centrifugation of blood samples at 3000 \times *g* for 15 minutes, and AST and ALT activities were measured using an Alanine Aminotransferase Assay Kit (C009-2-1; Nanjing Jiancheng Bioengineering Institute, Nanjing, China) and an Aspartate Aminotransferase Assay Kit (C010-2-1; Nanjing Jiancheng Bioengineering Institute, Nanjing, China) according to the manufacturer's instructions on a microplate reader at 510 nm.

Intracellular Antioxidant Capacity Evaluation

Liver SOD, GSH, and MDA levels were measured by a SOD assay kit (A001-3-2; Nanjing Jiancheng Bioengineering Institute), GSH assay kit (S0053; Beyotime, Shanghai, China), and a lipid peroxidation MDA assay kit (S0131; Beyotime) following the manufacturer's instructions. Absorbance values at 450 nm, 412 nm, and 535 nm were recorded separately, and SOD, GSH, and MDA levels were calculated from a standard curve.

Immunofluorescence Staining

Liver tissues were collected and routinely embedded in optimal cutting tissue. Frozen liver samples were sliced into 14- μ m sections. For immunofluorescence staining, after being washed with phosphate-buffered saline (PBS) 3 times, the sections were penetrated with methanol at -20°C for 10 minutes and sealed with 5% goat serum at room temperature for 1 hour. Finally, frozen liver sections were stained with CD68 (ab201340; Abcam, Cambridge, UK), CD11b (ab52478; Abcam), Ptgs2 (ab15191; Abcam), DMT1 (ab55812; Abcam), GPX4 (ab125066; Abcam), F4/80 (DF2789; Affinity, Jiangsu, China), TGF β 1 (ER31210; huabio, Hangzhou, China; 21898-1-AP; Proteintech), Ki67 (9129s; Cell Signaling Technology, Boston, MA), GSK3 β (9832s; Cell Signaling Technology), P-GSK3 β (5558p; Cell Signaling Technology), Nrf2 (16396-1; Proteintech, Chicago, IL), and iNOS (ab178945; Abcam) overnight at 4°C. After extensive washing, the frozen sections were incubated with the respective fluorescent secondary antibodies. Finally, the nucleus was stained with 4',6-diamidino-2-phenylindole for 10 minutes.

Immunochemical Staining

For immunochemical staining, paraffin sections (4 μ m) were first dewaxed in xylene I, II, and III, and then rehydrated in 100%, 95%, 90%, 80%, and 70% ethanol. Then, the samples were boiled in 1 \times sodium citrate, maintained at a boiling temperature for 10 minutes to repair antigen, and cooled to room temperature. Afterward, endogenous peroxidase enzyme was inactivated using 3% H₂O₂ in methanol for 10 minutes in the dark at room temperature. After blocking nonspecific binding with 5% goat serum at room temperature, the sections were stained with antibodies against F4/80, DMT1, Ptgs2, 4-HNE (MAB3249-SP; R&D, Minneapolis, MN), NT (9691S; Cell Signaling Technology), and TGF β 1 (ab31013; Abcam) overnight at 4°C. The next day, sections were incubated with the respective biotinylated secondary antibodies. Positive staining was visualized using diaminobenzidine (DAB). The reaction was stopped in ice water. Then, the samples were counterstained with hematoxylin, dehydrated, paraffinized, and finally mounted and sealed with neutral gum. The dyed sections were photographed with an optical microscope (Eclipse Ni-U; Nikon).

TUNEL Assay

The TUNEL reaction was used to detect hepatocyte apoptosis in liver tissue by using frozen sections and the In Situ Cell Death Detection Kit (Roche, Indianapolis, IN). The cryosections were immersed in 0.01% Triton X-100 (Sigma, Saint Louis, MO) diluted in PBS for 10 minutes, washed with

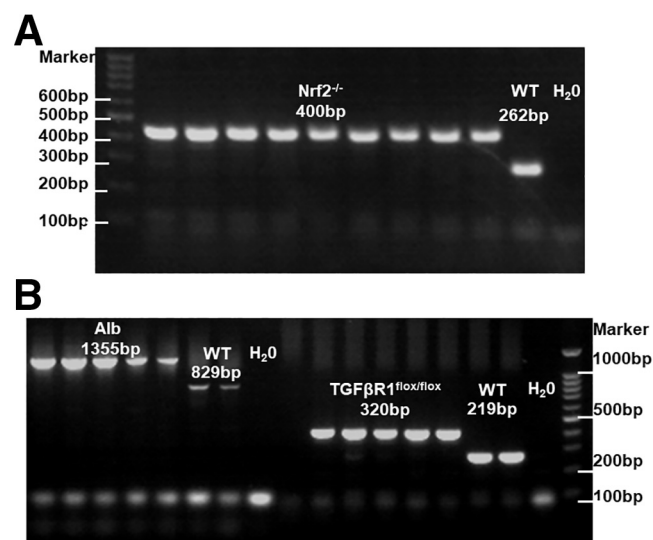


Figure 14. The gene identification results of *Nrf2*^{-/-}, *B6.129-Alb*^{m1(CreERT2)Srcmo}, and *TGF β 1*^{flox/flox} mice. (A) Gene identification results of *Nrf2*^{-/-} mice were validated according to the standard polymerase chain reaction (PCR) protocols posted on the Jackson Laboratory official website. (B) Gene identification results of *B6.129-Alb*^{m1(CreERT2)Srcmo} mice were validated according to the standard PCR protocols posted on the Shanghai Model Organism while *TGF β 1*^{flox/flox} mice were validated according to the standard PCR protocols posted on the Jackson Laboratory official website. Alb, Albumin.

PBS, incubated with a 1:10 TUNEL working solution in a dark environment at 37°C for 1 hour, and washed 3 times with PBS. Then, 4',6-diamidino-2-phenylindole was used to stain nuclei in the dark at room temperature for 5 minutes, and the samples were washed 3 times with PBS. The dyed cryosections were photographed immediately with an optical microscope (Eclipse Ni-U; Nikon).

Western Blot Analysis

Liver tissues were sonicated in ice-cold radioimmunoprecipitation lysis buffer (Beyotime, Shanghai, China) containing a phosphatase inhibitor cocktail (Beyotime, Shanghai, China) and a protease inhibitor cocktail (Beyotime, Shanghai, China). Protein concentrations were determined by a quantitative bicinchoninic acid (BCA) assay. A total of 20–30 μ g of protein was used for immunoblotting. Primary antibodies against GPX4 (1:5000, ab125066, Abcam), xCT (1:1000, ab37185; Abcam), Ptgs2 (1:1000, ab15191, Abcam), TFR (1:1000, ab84036; Abcam; 10084-2-AP; Proteintech), GSK3 β , P-GSK3 β , Nrf2, and iNOS (1:1000, ab178945; Abcam), Nrf2 (1:1000, 16396-1AP; Proteintech), TGF β 1 (1:1000, ab31013; Abcam), CHAC1 (1:1000, 15207-1-AP; Proteintech), DHODH (1:1000, 14877-1-AP; Proteintech), FSP1 (1:1000, 20886-1-AP; Proteintech), POR (1:1000, ab180597; Abcam), caspase 8 (1:1000, 4927S; Cell Signaling Technology), cleaved caspase 8 (1:1000, 8592S; Cell Signaling Technology), caspase 9 (1:1000, 9504S; Cell Signaling Technology), BCL2 (1:1000, sc-7382; Santa Cruz Biotechnology, Santa Cruz, CA), BAX (1:1000, sc-20067; Santa Cruz Biotechnology), RIP3 (1:1000, sc-374639; Santa Cruz Biotechnology), GSDMD (1:1000, ab209845; Abcam), β -actin (1:2000, T0022; Affinity), and glyceraldehyde-3-phosphate dehydrogenase (1:2000, 2118S; Cell Signaling Technology) were applied in the study.

Transmission Electron Microscopy

Liver tissues were fixed with 2.5% paraformaldehyde and 2.5% glutaraldehyde in Sorenson's phosphate buffer at pH 7.4. The liver tissues then were sectioned at 50 ~ 60 nm, and sections were placed on copper mesh grids. The sections were stained with uranyl acetate and lead citrate for contrast and examined with a transmission electron microscope (Hitachi H-7500, Tokyo, Japan).

Genotyping Experiments

The genotyping method was performed according to the standard PCR protocols posted on Jackson Laboratory's official website for JAX mice and Shanghai model organisms. The gene identification results of B6.129-Alb^{tm1(CreERT2)Srcmo}, TGF β 1^{flox/flox}, and Nrf2^{-/-} mice were validated and presented in Figure 14.

AAV Vector Generation and Delivery

AAV9-Nfe2l2-RNAi (105063-1) was designed, produced, and constructed by Shanghai Gene. The viral particle suspension was thawed, diluted with saline, and administered

via tail vein injection at a dose of 2×10^{11} vg per mouse. In the Nrf2-RNAi group, TGF β 1 ^{Δ hep-CKO} mice were injected with AAV9-Nfe2l2-RNAi. The NC group with the same number of TGF β 1 ^{Δ hep-CKO} mice was injected with the AAV9 negative virus. The next experiment was performed 3 weeks after the virus injection.

Statistical Analysis

The numeric results are shown as the means \pm SEM. All statistical analyses were performed with GraphPad Prism version 9.0 software (San Diego, CA) and SPSS 20.0. (Chicago, IL) One-way analysis of variance or an unpaired *t* test was used for statistical analysis, and the Dunnett T3 multiple comparisons test was used for the pairwise comparison of 3 or more samples. *P* values less than 0.05 were considered statistically significant.

Ethics Statement

This study did not include any human experiments. We certified that the use of all mice involved in this project, including the number of animals, species used, or procedures performed, were performed according to the provisions of the Animal Welfare Act, Public Health Service (PHS) Animal Welfare Policy, the principles of the National Institutes of Health Guide for the Care and Use of Laboratory Animals, and approved by the National Institutional Animal Care and Ethical Committee of Southern Medical University.

References

1. Tunon MJ, San Miguel B, Crespo I, Jorquera F, Santamaria E, Alvarez M, Prieto J, Gonzalez-Gallego J. Melatonin attenuates apoptotic liver damage in fulminant hepatic failure induced by the rabbit hemorrhagic disease virus. *J Pineal Res* 2011;50:38–45.
2. Mallick S, Nair K, Thillai M, Manikandan K, Sethi P, Madhusrinivasan D, Johns SM, Binoj ST, Mohammed Z, Ramachandran NM, Balakrishnan D, Unnikrishnan G, Dhar P, Sudheer OV, Sudhindran S. Liver transplant in acute liver failure - looking back over 10 years. *J Clin Exp Hepatol* 2020;10:322–328.
3. Tuñón MJ, Alvarez M, Culebras JM, González-Gallego J. An overview of animal models for investigating the pathogenesis and therapeutic strategies in acute hepatic failure. *World J Gastroenterol* 2009; 15:3086–3098.
4. Silverstein R. D-galactosamine lethality model: scope and limitations. *J Endotoxin Res* 2004;10:147–162.
5. Endo Y, Shibasaki M, Yamaguchi K, Kai K, Sugawara S, Takada H, Kikuchi H, Kumagai K. Enhancement by galactosamine of lipopolysaccharide(LPS)-induced tumour necrosis factor production and lethality: its suppression by LPS pretreatment. *Br J Pharmacol* 1999; 128:5–12.
6. Yan T, Huang J, Nisar MF, Wan C, Huang W. The beneficial roles of SIRT1 in drug-induced liver injury. *Oxid Med Cell Longev* 2019;2019:8506195.

7. Deng G, Li Y, Ma S, Gao Z, Zeng T, Chen L, Ye H, Yang M, Shi H, Yao X, Zeng Z, Chen Y, Song Y, Liu B, Gao L. Caveolin-1 dictates ferroptosis in the execution of acute immune-mediated hepatic damage by attenuating nitrogen stress. *Free Radic Biol Med* 2020; 148:151–161.
8. Zeng T, Deng G, Zhong W, Gao Z, Ma S, Mo C, Li Y, Huang S, Zhou C, Lai Y, Xie S, Xie Z, Chen Y, He S, Lv Z, Gao L. Indoleamine 2, 3-dioxygenase 1 enhances hepatocytes ferroptosis in acute immune hepatitis associated with excess nitrative stress. *Free Radic Biol Med* 2020;152:668–679.
9. Dixon SJ, Lemberg KM, Lamprecht MR, Skouta R, Zaitsev EM, Gleason CE, Patel DN, Bauer AJ, Cantley AM, Yang WS, Morrison B 3rd, Stockwell BR. Ferroptosis: an iron-dependent form of nonapoptotic cell death. *Cell* 2012;149:1060–1072.
10. Kuang F, Liu J, Tang D, Kang R. Oxidative damage and antioxidant defense in ferroptosis. *Front Cell Dev Biol* 2020;8:586578.
11. Yang WS, SriRamaratnam R, Welsch ME, Shimada K, Skouta R, Viswanathan VS, Cheah JH, Clemons PA, Shamji AF, Clish CB, Brown LM, Girotti AW, Cornish VW, Schreiber SL, Stockwell BR. Regulation of ferroptotic cancer cell death by GPX4. *Cell* 2014;156:317–331.
12. Bersuker K, Hendricks JM, Li Z, Magtanong L, Ford B, Tang PH, Roberts MA, Tong B, Maimone TJ, Zoncu R, Bassik MC, Nomura DK, Dixon SJ, Oltmann JA. The CoQ oxidoreductase FSP1 acts parallel to GPX4 to inhibit ferroptosis. *Nature* 2019;575:688–692.
13. Mao C, Liu X, Zhang Y, Lei G, Yan Y, Lee H, Koppula P, Wu S, Zhuang L, Fang B, Poyurovsky MV, Olszewski K, Gan B. DHODH-mediated ferroptosis defence is a targetable vulnerability in cancer. *Nature* 2021; 593:586–590.
14. Ying W, Wu YL, Feng XC, Lian LH, Jiang YZ, Nan JX. The protective effects of total saponins from *Ornithogalum saundersiae* (Liliaceae) on acute hepatic failure induced by lipopolysaccharide and D-galactosamine in mice. *J Ethnopharmacol* 2010;132:450–455.
15. Yamada N, Karasawa T, Kimura H, Watanabe S, Komada T, Kamata R, Sampilvanjil A, Ito J, Nakagawa K, Kuwata H, Hara S, Mizuta K, Sakuma Y, Sata N, Takahashi M. Ferroptosis driven by radical oxidation of n-6 polyunsaturated fatty acids mediates acetaminophen-induced acute liver failure. *Cell Death Dis* 2020;11:144.
16. Xu D, Xu M, Jeong S, Qian Y, Wu H, Xia Q, Kong X. The role of Nrf2 in liver disease: novel molecular mechanisms and therapeutic approaches. *Front Pharmacol* 2018; 9:1428.
17. Jiang Y, Bao H, Ge Y, Tang W, Cheng D, Luo K, Gong G, Gong R. Therapeutic targeting of GSK3beta enhances the Nrf2 antioxidant response and confers hepatic cytoprotection in hepatitis C. *Gut* 2015;64:168–179.
18. Massague J. TGFbeta signalling in context. *Nat Rev Mol Cell Biol* 2012;13:616–630.
19. Miwa Y, Harrison PM, Farzaneh F, Langley PG, Williams R, Hughes RD. Plasma levels and hepatic mRNA expression of transforming growth factor-beta1 in patients with fulminant hepatic failure. *J Hepatol* 1997; 27:780–788.
20. McMillin M, Galindo C, Pae HY, Frampton G, Di Patre PL, Quinn M, Whittington E, DeMorrow S. Gli1 activation and protection against hepatic encephalopathy is suppressed by circulating transforming growth factor beta1 in mice. *J Hepatol* 2014;61:1260–1266.
21. Bird Thomas G, Müller M, Boulter L, et al. TGFβ inhibition restores a regenerative response in acute liver injury by suppressing paracrine senescence. *Sci Transl Med* 2018;1230:1–14.
22. Antoniadou CG, Berry PA, Wendon JA, Vergani D. The importance of immune dysfunction in determining outcome in acute liver failure. *J Hepatol* 2008; 49:845–861.
23. Jaeschke H, Fisher MA, Lawson JA, Simmons CA, Farhood A, Jones DA. Activation of caspase 3 (CPP32)-like proteases is essential for TNF-α-induced hepatic parenchymal cell apoptosis and neutrophil-mediated necrosis in a murine endotoxin shock model. *J Immunol* 1998;160:3480–3486.
24. Li Y, Cao Y, Xiao J, Shang J, Tan Q, Ping F, Huang W, Wu F, Zhang H, Zhang X. Inhibitor of apoptosis-stimulating protein of p53 inhibits ferroptosis and alleviates intestinal ischemia/reperfusion-induced acute lung injury. *Cell Death Differ* 2020;27:2635–2650.
25. Xie Y, Hou W, Song X, Yu Y, Huang J, Sun X, Kang R, Tang D. Ferroptosis: process and function. *Cell Death Differ* 2016;23:369–379.
26. Salazar M, Rojo AI, Velasco D, de Sagarra RM, Cuadrado A. Glycogen synthase kinase-3beta inhibits the xenobiotic and antioxidant cell response by direct phosphorylation and nuclear exclusion of the transcription factor Nrf2. *J Biol Chem* 2006; 281:14841–14851.
27. Dodson M, Castro-Portuguez R, Zhang DD. NRF2 plays a critical role in mitigating lipid peroxidation and ferroptosis. *Redox Biol* 2019;23:101107.
28. Rodgers SK, Horrow MM. Acute (fulminant) liver failure: a clinical and imaging review. *Abdom Radiol (NY)* 2021; 46:3117–3127.
29. Dong V, Nanchal R, Karvellas CJ. Pathophysiology of acute liver failure. *Nutr Clin Pract* 2020;35:24–29.
30. Maes M, Vinken M, Jaeschke H. Experimental models of hepatotoxicity related to acute liver failure. *Toxicol Appl Pharmacol* 2016;290:86–97.
31. Niu B, Lei X, Xu Q, et al. Protecting mitochondria via inhibiting VDAC1 oligomerization alleviates ferroptosis in acetaminophen-induced acute liver injury. *Cell Biol Toxicol* 2021:1–26, Epub ahead of print.
32. Wang C, Liu T, Tong Y, Cui R, Qu K, Liu C, Zhang J. Ulinastatin protects against acetaminophen-induced liver injury by alleviating ferroptosis via the SIRT1/NRF2/HO-1 pathway. *Am J Transl Res* 2021; 13:6031–6042.
33. Zhong X, Zhang Z, Shen H, Xiong Y, Shah YM, Liu Y, Fan XG, Rui L. Hepatic NF-κB-inducing kinase and inhibitor of NF-κB kinase subunit α promote liver oxidative stress, ferroptosis, and liver injury. *Hepatol Commun* 2021;5:1704–1720.

34. Jaeschke H, Adelusi OB, Ramachandran A. Ferroptosis and acetaminophen hepatotoxicity: are we going down another rabbit hole? *Gene Expr* 2021;20:169–178.
35. Leist M, Gantner F, Jilg S, Wendel A. Activation of the 55 kDa TNF receptor is necessary and sufficient for TNF-induced liver failure, hepatocyte apoptosis, and nitrite release. *J Immunol* 1995;154:1307–1316.
36. Bajt ML, Vonderfecht SL, Jaeschke H. Differential protection with inhibitors of caspase-8 and caspase-3 in murine models of tumor necrosis factor and Fas receptor-mediated hepatocellular apoptosis. *Toxicol Appl Pharmacol* 2001;175:243–252.
37. Ahmedy OA, Salem HH, Sayed NH, Ibrahim SM. Naringenin affords protection against lipopolysaccharide/D-galactosamine-induced acute liver failure: role of autophagy. *Arch Biochem Biophys* 2022;717:109121.
38. Ding K, Li X, Ren X, Ding N, Tao L, Dong X, Chen Z. GBP5 promotes liver injury and inflammation by inducing hepatocyte apoptosis. *FASEB J* 2022;36:e22119.
39. Li R, Yang W, Yin Y, Zhang P, Wang Y, Tao K. Protective role of 4-Octyl itaconate in murine LPS/D-GalN-induced acute liver failure via inhibiting inflammation, oxidative stress, and apoptosis. *Oxid Med Cell Longev* 2021;2021:9932099.
40. Zhang X, Ge J, Zhu X, Zhang H, Wang Y, Xu T, Jiang W, Zhang B. Effects and mechanism of oxymatrine combined with compound yinchen granules on the apoptosis of hepatocytes through the Akt/FoxO3a/Bim pathway. *Biomed Res Int* 2022;2022:8644356.
41. Liu M, He J, Zheng S, Zhang K, Ouyang Y, Zhang Y, Li C, Wu D. Human umbilical cord mesenchymal stem cells ameliorate acute liver failure by inhibiting apoptosis, inflammation and pyroptosis. *Ann Transl Med* 2021;9:1615.
42. Yang W, Tao K, Zhang P, Chen X, Sun X, Li R. Maresin 1 protects against lipopolysaccharide/d-galactosamine-induced acute liver injury by inhibiting macrophage pyroptosis and inflammatory response. *Biochem Pharmacol* 2022;195:114863.
43. Zhan Z, Zhang T, Dai F, Wen X, Chen Y, Jiang H, Gu T, Cheng Y, Tang L. Effect of oridonin on oxylipins in the livers of mice with acute liver injury induced by D-galactosamine and lipopolysaccharide. *Int Immunopharmacol* 2022;102:108387.
44. Ji Y, Si W, Zeng J, Huang L, Huang Z, Zhao L, Liu J, Zhu M, Kuang W. Niujiaodihuang detoxify decoction inhibits ferroptosis by enhancing glutathione synthesis in acute liver failure models. *J Ethnopharmacol* 2021;279:114305.
45. Siregar AS, Nyiramana MM, Kim EJ, Cho SB, Woo MS, Lee DK, Hong SG, Han J, Kang SS, Kim DR, Choi YJ, Kang D. Oyster-derived Tyr-Ala (YA) peptide prevents lipopolysaccharide/D-galactosamine-induced acute liver failure by suppressing inflammatory, apoptotic, ferroptotic, and pyroptotic signals. *Mar Drugs* 2021;19:614.
46. Wang Y, Chen Q, Shi C, Jiao F, Gong Z. Mechanism of glycyrrhizin on ferroptosis during acute liver failure by inhibiting oxidative stress. *Mol Med Rep* 2019;20:4081–4090.
47. Karki R, Sharma BR, Tuladhar S, Williams EP, Zalduondo L, Samir P, Zheng M, Sundaram B, Banoth B, Malireddi RKS, Schreiner P, Neale G, Vogel P, Webby R, Jonsson CB, Kanneganti TD. Synergism of TNF-alpha and IFN-gamma triggers inflammatory cell death, tissue damage, and mortality in SARS-CoV-2 infection and cytokine shock syndromes. *Cell* 2021;184:149–168 e17.
48. Ma K, Zhang Y, Zhu D, Lou Y. Protective effects of Asiatic acid against D-galactosamine/lipopolysaccharide-induced hepatotoxicity in hepatocytes and Kupffer cells co-cultured system via redox-regulated leukotriene C4 synthase expression pathway. *Eur J Pharmacol* 2009;603:98–107.
49. Gujral JS, Hinson JA, Farhood A, Jaeschke H. NADPH oxidase-derived oxidant stress is critical for neutrophil cytotoxicity during endotoxemia. *Am J Physiol Gastrointest Liver Physiol* 2004;287:G243–G252.
50. Chowdhury A, Nabila J, Adelusi Temitope I, Wang S. Current etiological comprehension and therapeutic targets of acetaminophen-induced hepatotoxicity. *Pharmacol Res* 2020;161:105102.
51. Ren F, Zhou L, Zhang X, Wen T, Shi H, Xie B, Li Z, Chen D, Wang Z, Duan Z. Endoplasmic reticulum stress-activated glycogen synthase kinase 3beta aggravates liver inflammation and hepatotoxicity in mice with acute liver failure. *Inflammation* 2015;38:1151–1165.
52. Wei L, Ren F, Zhang X, Wen T, Shi H, Zheng S, Zhang J, Chen Y, Han Y, Duan Z. Oxidative stress promotes D-GalN/LPS-induced acute hepatotoxicity by increasing glycogen synthase kinase 3beta activity. *Inflamm Res* 2014;63:485–494.
53. Niture SK, Khatri R, Jaiswal AK. Regulation of Nrf2-an update. *Free Radic Biol Med* 2014;66:36–44.
54. Jain AK, Jaiswal AK. GSK-3beta acts upstream of Fyn kinase in regulation of nuclear export and degradation of NF-E2 related factor 2. *J Biol Chem* 2007;282:16502–16510.
55. Cuadrado A. Structural and functional characterization of Nrf2 degradation by glycogen synthase kinase 3/beta-TrCP. *Free Radic Biol Med* 2015;88:147–157.
56. Eguchi S, Kamlot A, Ljubimova J, Hewitt WR, Lebow LT, Demetriou AA, Rozga J. Fulminant hepatic failure in rats: survival and effect on blood chemistry and liver regeneration. *Hepatology* 1996;24:1452–1459.
57. Michaeloudes C, Sukkar MB, Khorasani NM, Bhavsar PK, Chung KF. TGF-beta regulates Nox4, MnSOD and catalase expression, and IL-6 release in airway smooth muscle cells. *Am J Physiol Lung Cell Mol Physiol* 2011;300:L295–L304.
58. Gruppiso PA, Mikumo R, Brautigan DL, Braun L. Growth arrest induced by transforming growth factor-beta 1 is accompanied by protein phosphatase activation in human keratinocytes. *J Biol Chem* 1991;266:3444–3448.
59. King TD, Gandy JC, Bijur GN. The protein phosphatase-1/inhibitor-2 complex differentially regulates GSK3 dephosphorylation and increases sarcoplasmic/endoplasmic reticulum calcium ATPase 2 levels. *Exp Cell Res* 2006;312:3693–3700.

Received July 27, 2021. Accepted February 11, 2022.

Correspondence

Corresponding author address: Lei Gao, ZhuJiang Hospital of Southern Medical University, Guangzhou, Guangdong, 510285, China. e-mail: raygaolei@smu.edu.cn; OR Guangdoeng Provincial Key Laboratory of Shock and Microcirculation, Southern Medical University, Guangzhou, 510515, China e-mail: hstcm@126.com; OR Shaohui Huang, Zhiping Lv, School of Traditional Chinese Medicine, Southern Medical University, Guangzhou, Guangdong, 510515, China. e-mail: hstcm2018@163.com; lzp48241@126.com.

Acknowledgments

The authors thank Mr Zhitao Zhou and Ms Yanmeng Lu (Central Laboratory, Southern Medical University, Guangzhou, China) for their technical assistance.

CRediT Authorship Contributions

Lv Zhiping (Supervision: Lead)
Sha Huang (Conceptualization: Equal; Writing – original draft: Lead)
Yuhua Wang (Conceptualization: Equal)
Shunwen Xie (Methodology: Equal)
Yuqi Lai (Data curation: Equal)
Chan Mo (Formal analysis: Equal)

Ting Zeng (Software: Equal)
Shanshan Kuang (Validation: Equal)
Guanghui Deng (Validation: Equal)
Chuying Zhou (Writing – review & editing: Supporting)
Yuyao Chen (technical support: Supporting)
Shaohui Huang (Funding acquisition: Supporting)
Lei Gao (Conceptualization: Equal; Funding acquisition: Supporting; Investigation: Equal)
Zhiping Lv (Funding acquisition: Lead; Project administration: Lead)

Conflicts of interest

The authors disclose no conflicts.

Funding

This project was financially supported by the National Natural Science Foundation of China (82174168, 81774170, 82074131, 81603501, and 81673774), the Natural Science Foundation of Guangdong Province (2018B030306012, 2021A1515011667), the Scientific Research Initiative Program of Southern Medical University (CX2017N001), the Outstanding Youth Development Scheme project of Southern Medical University (G621299870), and the Shenzhen Guangming District health system research project (2020R01126).